Tin Oxide Sensors for Insect Infestation Detection

by

Junpin Teng

A thesis submitted to the Graduate Faculty of
Auburn University
in partial Fulfillment of the
requirements for the Degree of
Master of Science

Auburn, Alabama
December 18, 2009

Approved by

Bryan A. Chin, Chair, Professor of Materials Engineering
Zhongyang Cheng, Associate Professor of Materials Engineering
Jong Wook Hong, Associate Professor of Materials Engineering
Arnold Vainrub, Associate Professor of Anatomy, Physiology and Pharmacology

Abstract

Agriculture suffers a significant loss every year due to pests. Early detection of insect infestation is important to reduce that kind of loss. Plants emit volatile organic compounds whose composition will change after the infestation of pests. Detection of such change can provide the critical information for pest control. In this research thick film hotplate type tin oxide sensors are used to detect Methyl Jasmonate, an important plants' defense relating volatile chemical. The tests are performed by a gas flowing system. For the concentration dependence study of the sensors different partial flow rate (0.02L/min, 0.04L/min, 0.06L/min, 0.08L/min, 0.10L/min, 0.12L/min, 0.16L/min, 0.20L/min) of Methyl Jasmonate at 25°C in dry air flow is tested. Gas chromatography is used to determine the exact concentration of Methyl Jasmonate at different partial flow rate. The sensors' relative sensitivity is found to be from 2 to 5 and follow the power law relationship with the concentration of Methyl Jasmonate. For the temperature dependence study of the sensors the tests are performed in dry air flow at different temperature (-22°C, -12°C, -2°C, 7°C, 17°C, 22°C, 27°C, 32°C, 37°C). The sensor's relative sensitivity is found to be relatively low about 4 around 20°C and increases with decreasing ambient temperature below 10°C. For humidity dependence study the tests are performed at 25°C with different relative humidity (20%, 64%, 70%, 82%, 94%). The relative sensitivity of the sensor is decreasing with increasing relative humidity, but still above 3 in high relative humidity. According to the performance of the sensors to different concentration of

Methyl Jasmonate at different temperature and relative humidity the capability of tin oxide sensors in detecting insect infestation is discussed.

Acknowledgements

The author would like to thank Dr. Bryan Chin for advisement and thank research group members (Suiqiong Li, Shichu Huang, Wen Shen, John Shu, Shin Horikawa, Kanchana Weerakoon) for help during the research. Thanks are also to my family members especially my wife Jun Lu for the support during the course of investigation.

Table of Contents

List of Tables

List of Figures

CHAPTER 1: INTRODUCTION

The World Food and Agriculture Organization of the United Nations (FAO) estimates that the annual loss of edible food plants due to pests is about 14%. This is equivalent to more than $200 billion dollars in economic loss every year. In the USA, one third of all agriculture products are damaged by pests which leads to an average annual economic loss of over $4 billion [1]. Hence early detection of insect pests could significantly reduce current economic losses.

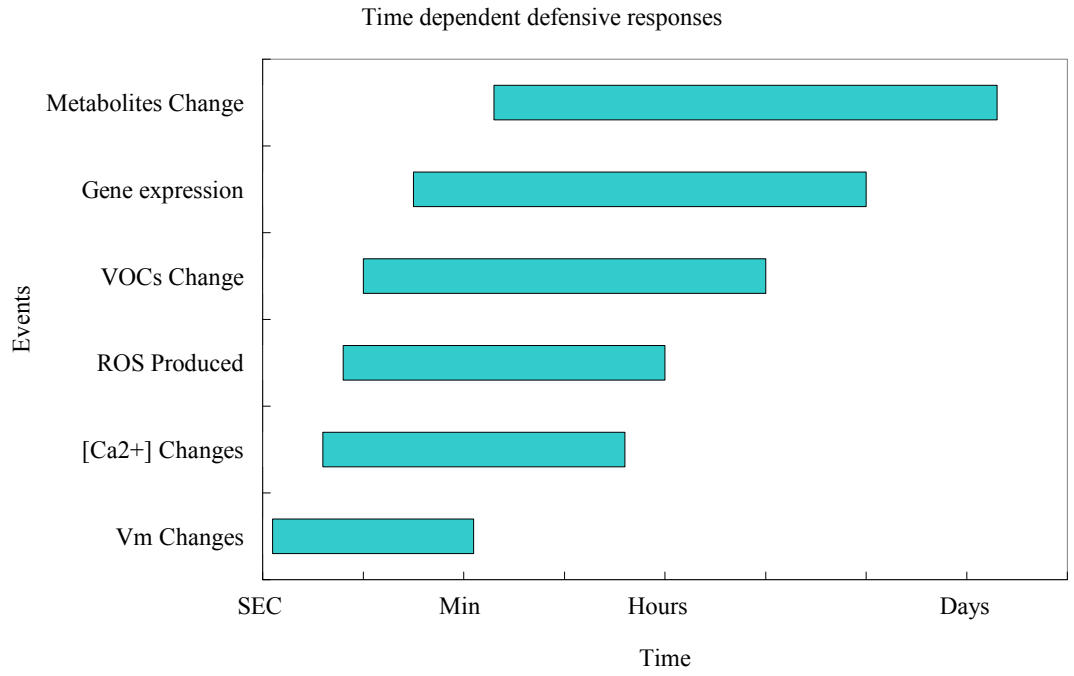

Figure 1: Plants' time dependent defensive responses

Plants have a natural phytochemical defense system that is activated by invading herbivores. After being attacked by herbivores, plants have a series of responses at

different time stages (Fig 1) [2]. The chain responses start from the plasma membrane of plant cells which directly contact the environment. Seconds after herbivores' attack plants the plasma transmembrane potential (Vm) changes [3]. Vm is directly influenced by ion influxes among which Ca^{2+} is predominant in cell signaling and recognized as an important second messenger [4]. Following the Ca^{2+} concentration change, reactive oxygen species (ROS) such as H_2O_2 are increasingly produced. At low concentration ROS also acts as secondary messengers [5-6]. As the level of ROS increases when the insects' attack persist ROS especially H_2O_2 can defend a plant's wounded area from further invasion of bacteria, fungi, or viruses [7]. After ROS changes volatile organic compounds (VOC) emitted by the plants change. VOC have a significant role in the plants' defense system which will be explicated later. Regulated by the network of phytohormones, the process of plants' biosynthesis changed. As a result the composition of plants' metabolites changes. Many secondary metabolites which usually act as a toxin to herbivores are produced to directly defend plants from the herbivores' invasion [8-10].

To communicate with the environment, plants emit hundreds of volatile organic compounds. At present more than 1700 kinds of VOC are identified from various plant families [11]. These chemical substances can not only regulate processes of growth and reproduction but also defend plants from herbivore's attack or deal with physical stress [12]. When plants are fed on by herbivores they will emit a different mixture of VOC blend. The difference of the mixture from normal conditions can be quantitative or qualitative. Quantitative difference is the relative composition ratio change of VOC mixture emitted by plants after and before a herbivore's infestation. Qualitative difference is due to new kinds of VOC that are produced by plants after an insects' attack.

The VOC emitted by infested plants can defend against herbivores in three major ways. First, some VOC can directly repel insects [13-14]. Second, some VOC can attract natural predators of herbivores or egg parasitoids [15-19]. Therefore, the population of herbivores can be reduced to prevent plants from being overtaken. Third, some VOC can warn neighboring plants to activate their defense system [20-25]. Those VOC can trigger the biosynthesis of plant secondary metabolites which usually act as a toxin or inhibitors of insect digestive enzymes [8-10, 26-28]. Thus, neighboring plants can avoid or deter the future feeding of insects.

Among the many VOC, one family named jasmonates which is composed of Jasmonic acid (JA) and its derivatives should be noticed. These compounds will change quantitatively or qualitatively at the early stage of VOC changes that are observed minutes after plants being damaged by herbivores [29]. And they have intimate relationship with the plants' defense system. On one hand, they are important components in systemic wound signaling. Farmer et al discovered that local treatment of jasmonates can activate the systemic expression of wound response genes. Based on this finding jasmonates are proposed as an important signaling VOC [30]. Later this hypothesis was substantiated by famous grafting experiments conducted by Li et al [31]. On the other hand, jasmonates play an integral role in crosstalk between signaling networks [32]. The jasmonate's signaling pathway interacts with many other signaling pathways such as ethylene, light, auxin, salicylic acid, and abscisic acid [33-37]. MeJa is a volatile counterpart of JA which is converted from JA by JA carboxyl methyltransferase (JMT) [38]. MeJa is vital substance in plants and is proposed as a strong candidate for an important role in systemic signaling [39]. It can diffuse to distal parts of the plant in vapor phase and activate formation of defense proteins, stress protective proteins, and thicker cell wall [40, 41]. When the plants are

infested the emission of Methyl Jasmonate the volatile counterpart of JA increases 40 fold to the concentration of several ppm [42]. Thus, it can be used to identify the early stages of an insect infestation. Once detected, appropriate treatment can be carried out in time to control the insects and prevent further loss.

The metal oxide sensor is one kind of conductometric sensor. Conductometric sensors have a significant portion of the commercial gas sensor market. SnO_2 is one of the most commonly used materials in metal oxide sensors. Metal oxide sensors have the merits of high sensitivity, quick response and low cost. Metal oxide sensors have been used to detect a wide range of gas species such as CO, H_2, CH_4, H_2S, NO_X, CO_2, and O_2 [43-73]. However, there has been no investigation involving detection of Methyl jasmonate and other gases emitted by a plants' phytochemical defense system. Hence, there is a demand to identify the capability of tin oxide sensors in detecting volatile organic compounds for the application of insect infestation detection. This thesis will investigate the performance of the tin oxide sensor in the detection of insect infestation.

CHAPTER 2: LITERATURE REVIEW

2.1. Review of current technologies for gas detection

There are many sensing technologies that may be used to detect Methyl Jasmonate the volatile counterpart of Jasmonic acid. Different principles that may be used for detection are summarized in Figure 2. The following are the discussions on different types of gas sensors.

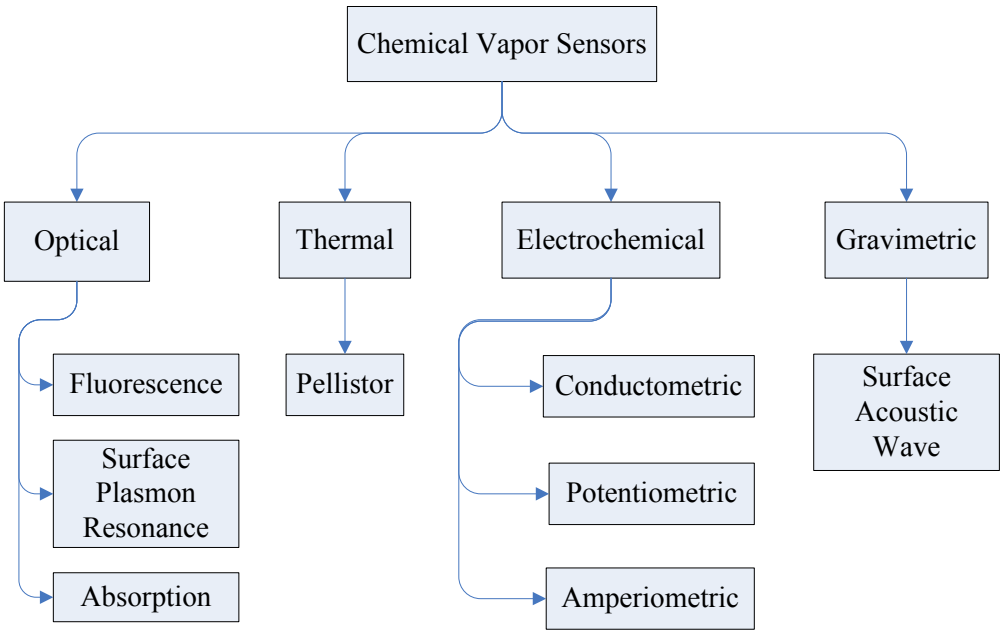

Figure 2: Different types of chemical vapor sensors.

2.1.1. Optical gas sensor

There are various types of optical gas sensors based on one or more different

optical phenomena (1) Fluorescence (2) Surface Plasmon Resonance (SPR) (3) Absorption. Fluorescence is the emission of photons by molecules after being electronicly excited by absorbing light. Figure 3 illustrates a typical gas sensor based on fluorescence. After the fluorescence material absorbs the excitation light it will emit a light with longer wavelength which is the fluorescence signal. In the presence of target gas the fluorescence intensity emitted by fluorescence material will change due to interaction between the gas and the sensing material. Hence, the gas concentration can be related to the fluorescence intensity F as:

$$C = K\left(\frac{F - F_{\min}}{F_{\max} - F}\right) \qquad (1)$$

where C is concentration of the target gas, $F_{\min}$ is fluorescence intensity without presence of target gas, $F_{\max}$ is fluorescence intensity when the fluorescence material is saturated by target gas. This kind of sensor has high sensitivity and wide detection range. The major problem with this type of sensor is durability due to the degrading of the fluorescence material which also reduces the sensitivity and accuracy of the sensor [75].

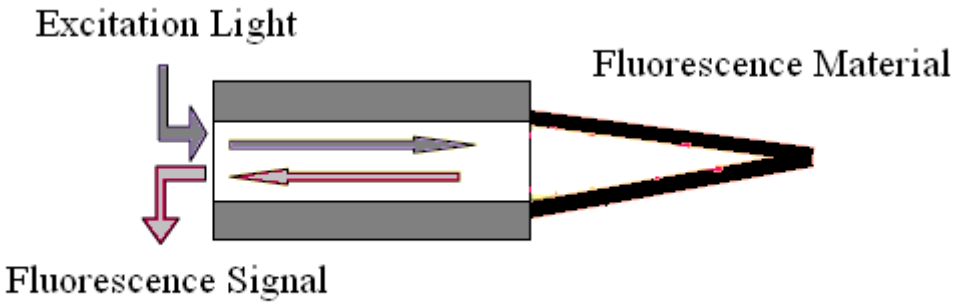

Figure 3: Schematic of a fluorescence gas sensor [74]

Surface Plasmon resonance (SPR) sensors are a second type of optical sensor

that can be used for gas detection. Surface plasmon is a charge-density oscillation which may occur at the boundary of two media with opposite sign dielectric constants. It can be considered as an electromagnetic wave propagating along the surface in transverse magnetic mode. Figure 4 is a typical gas sensor based on SPR. When the component of a light's wave vector which is parallel to the interface matches the propagation constant of the surface plasmon, SPR occurs. The energy will transfer from the incident light to surface plasmon, so the intensity of reflected light decreases. At a certain angle θ_{SPR} the intensity of reflected light is reduced to minimum. After target gas interacting with the binding layer the surface condition of the metal layer changes. As a result θ_{SPR} changes which can be used for detection. This type of gas sensor is easy to use and extremely sensitive. However, it is bulky, expensive and mainly used in laboratories [76].

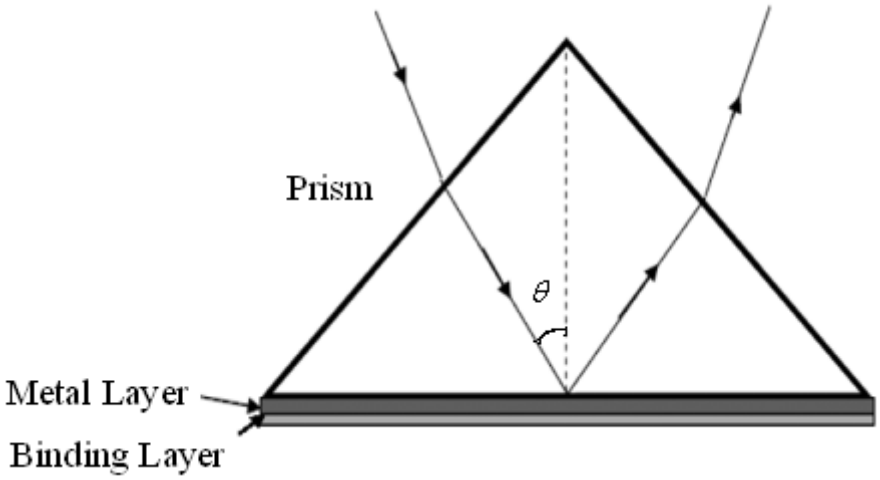

Figure 4: Schematic of a SPR based gas sensor [76].

Figure 5 is a typical gas sensor based on the light absorption by the gas. When white light passes through gases it will be absorbed at different extent at different wavelengths; each specific gas has its own light absorption spectrum which can be

used to discriminate the gases. Based on the Beer–Lambert law, the light intensity of the sensor can be related to target gas concentration as,

$$\frac{I}{I_0} = e^{-\varepsilon \cdot l \cdot c} \qquad (2)$$

where I is the transmitted intensity of the light after absorption, I_0 is the incident intensity of the light before absorption, ε is the absorptivity of the gas species, l is the optical path length and c is the concentration of the gas species. The merits of this kind of sensor are high sensitivity and selectivity. The disadvantages are relatively long response time and high cost. Though optical fibers can make the system more cost effective, it limits the working wavelength range; consequently, limiting the gas species that can be detected [74].

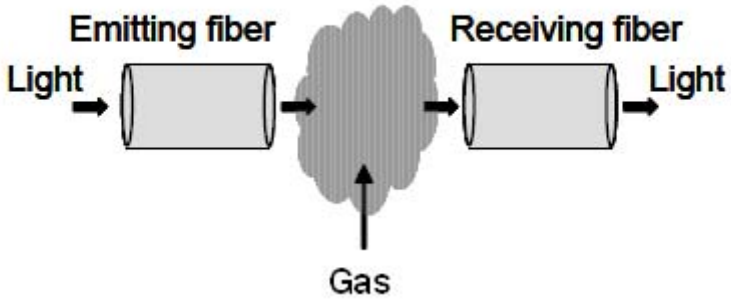

Figure 5: Schematic of an infrared absorption optical gas sensor [74].

2.1.2. Thermal gas sensor

Pellistor is the major kind of thermal gas sensor. It consists of a platinum wire coil in an alumina bead covered with a thick film catalyst, which is normally palladium [77]. Gas is combusted by electrically heating the catalyst material to the required temperature (about 500 °C) with the platinum wire. As a result the temperature increases due to oxidation of the combustible gas and is measured in

terms of the platinum resistance relative to a reference resistance. The resistance change is related to the concentration of the gas. This type of gas sensor is not widely used due to high power consumption and poisoning of catalyst material by sulfur compounds [78].

2.1.3. Electrochemical gas sensor

There are three major kinds of electrochemical gas sensors (1) Conductometric; (2) Potentiometric and (3) Amperometric. Conductometric gas sensors are usually fabricated as a chemiresistor as shown in Figure 6. The sensing element of the chemiresistor is conducting polymer or semiconductor. When the sensing element is exposed to the target gas the conductance (inverse resistance) of the sensor changes from that measured in normal air due to the adsorption of target gas. Hence the conductance (inverse resistance) change can be related to the gas concentration. This type of gas sensor has high sensitivity, quick response and good stability. The main drawback is poor selectivity [79-80].

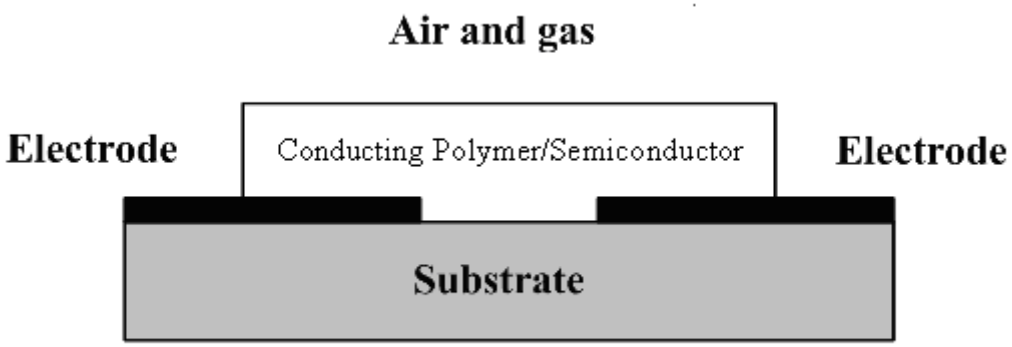

Figure 6: Schematic of conductometric gas sensor.

Figure 7 illustrates the conventional potentiometric gas sensor. Due to the gas concentration difference between the sensing (working) electrode side and reference

electrode side there is an electrochemical potential difference that develops between the electrodes (emf). Based on the Nernst law the open circle voltage measured between the electrodes can be related to the gas concentration as,

$$E = k \ln \frac{p}{p_0} \qquad (3)$$

where E is the potential measured, k is constant, p is the partial pressure of target gas which needs to be detected, p_0 is the partial pressure of gas concentration which is known. This type of gas sensor is highly sensitive and selective, but lacks long term stability. Moreover it is restricted to detect the gas which corresponds to the mobile ionic species in the electrolyte. Auxiliary electrodes can be added to detect other gases. However the complexity and cost of the system is increased [81-82].

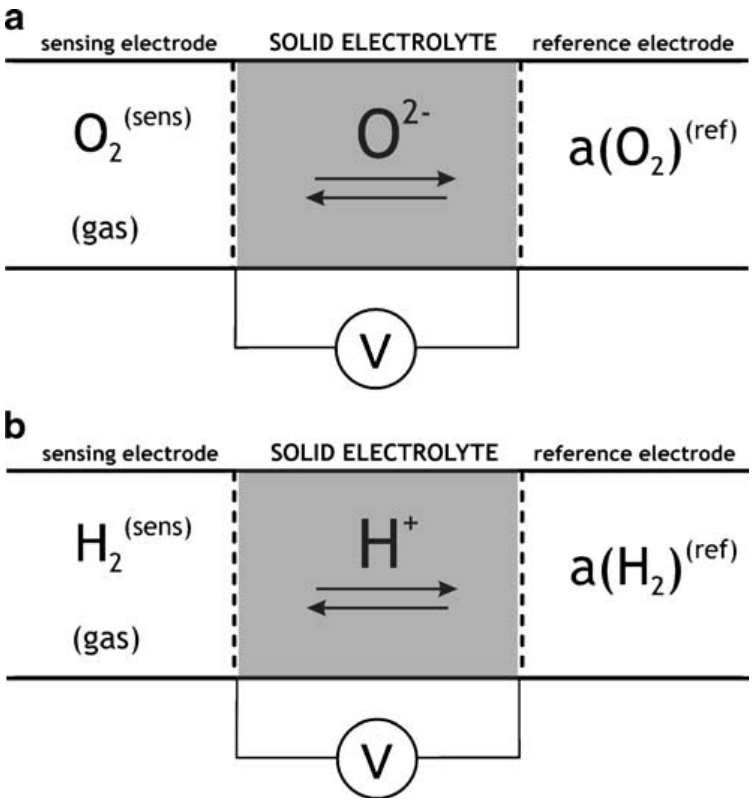

Figure 7: Schematic of conventional potentiometric gas sensor with (a) oxygen conductor (b) protonic conductor [81].

Figure 8 is a schematic of an amperometric gas sensor. After introduction of analyte gas the membrane will allow the target gas to diffuse into the membrane and effectively prevent the diffusion of other unwanted gases. The reference electrode is used to maintain the sensing electrode at a known electrochemical potential. By applying a constant potential between the working electrode and the reference electrode, the electroactive species of electrolyte will participate in electrochemical reaction. A reduction reaction occurs at the cathode while an oxidation reaction occurs at the anode. Thus, a current flow is established. Based on Faraday's law the relationship between the current flow of the circuit and gas concentration can be expressed as,

$$i = kp \qquad (4)$$

where k is constant, p is the gas concentration. This kind of gas sensor has good sensitivity and selectivity but has relatively long response time and is poor in long term stability [83].

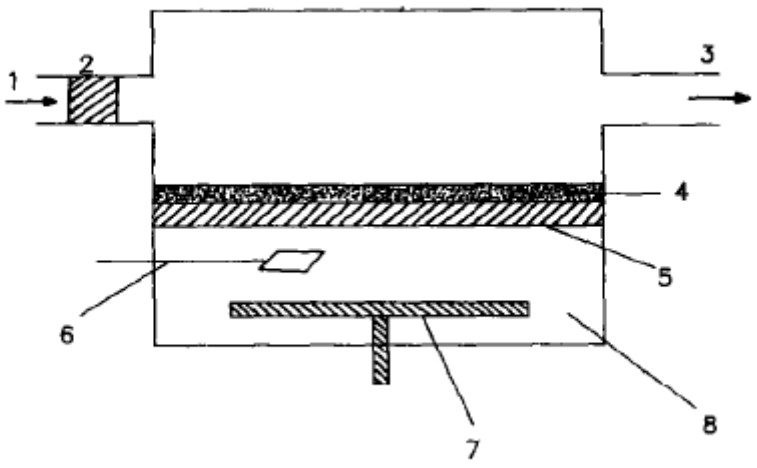

1. Gas inlet 2. Gas filter 3. Gas outlet 4. Gas membrane 5. Working electrode 6. Reference electrode 7. Counter electrode 8. Electrolyte

Figure 8: Schematic of an amperometric gas sensor [83].

2.1.4. Gravimetric gas sensor

The surface acoustic wave (SAW) sensor is the dominate gravimetric sensor used in gas detection. As shown in Figure 9 a SAW system is usually constructed on a piezoelectric substrate. The interdigitated transducer is used to generate a SAW. The SAW, first discovered by Lord Rayleigh, can couple with any media contacting the surface. Hence, when target gas is adsorbed or absorbed on the selective coating at the surface of the substrate, the amplitude and velocity of the SAW will change. Such a change can be interpreted by the receiving oscillator in terms of frequency shift which can be expressed as:

$$\Delta f = -Kf_0^2 \Delta m \qquad (5)$$

where Δf is the frequency shift, K is a constant, f_0 is the resonant frequency, and Δm is the mass change. This kind of sensor has the merits of high sensitivity, rapid response, low cost and small size. The main challenge comes from the sensing film which is coated on to the surface. The sensor response is dependent on film thickness, so the deviation of film thickness significantly affects the reproducibility of the sensor. Also the interaction between specific molecules and the sensing film changes the viscoelasticity which affects the sensor response [85].

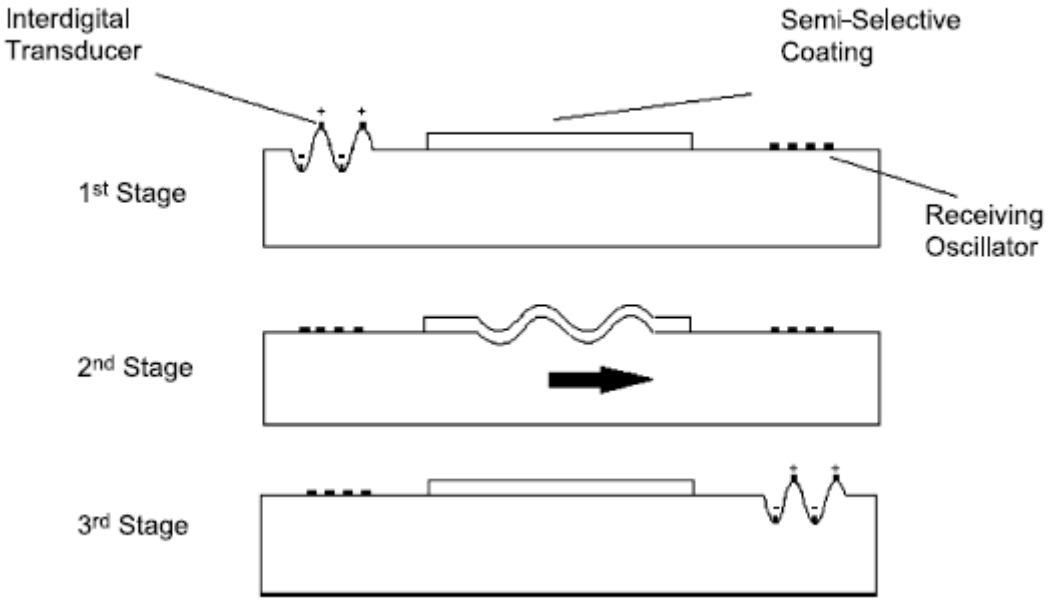

Figure 9: Schematic of a surface acoustic wave gas sensor [84].

Among the many different gas sensors discussed above, four types, (1) infrared absorption (optical); (2) electrochemical sensors (potentiometric or amperometric); (3) conducting polymer (conductometric) and (4) semiconductors (conductometric) are most attractive in gas detecting [86]. In practical use many features of gas sensors should be considered to fulfill the specific requirements. The final goal of this research project is to establish a remote monitoring system for plant health which is illustrated in Figure 4. The in field sensing system will detect the VOC emitted by plants and send the data to a host computer wirelessly. By analyzing the data, the in-situ plants' health condition will be monitored. The semiconductor gas sensor has merits of good sensitivity, quick response and high durability. Moreover, it is easy to combine the sensing element, signal converter, control electronics and other required electronics in one device [87]. Therefore, according to the comparison of the four popular gas sensors [88] shown in table 1 the semiconductor gas sensor, which will be described in detail later, was selected for this research. For this study tin oxide sensor

model TGS2620, manufactured by Figaro Inc., was investigated.

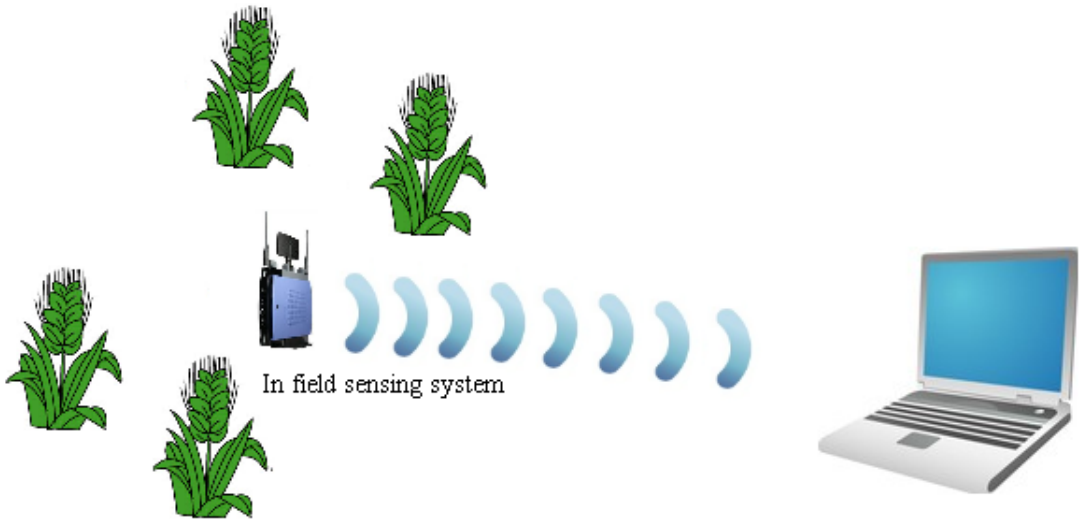

Figure 10: Schematic of the remote monitoring system for plants' health.

Table 1: Comparison of different types of gas sensors.

Parameter	Type of gas sensors			
	Semiconductor	Conducting Polymer	Electrochemical	Infrared Absorption
Sensitivity	e	e	g	e
Accuracy	g	g	g	e
Selectivity	p	p	g	e
Response time	e	e	p	p
Stability	g	g	b	g
Durability	g	b	p	e
Maintenance	e	g	g	p
Cost	e	e	g	b

e: excellent; g: good; p: poor; b: bad

2.2. Fundamentals of tin oxide semiconductor gas sensor

2.2.1. Gas-solid surface adsorption mechanism

When gas atoms or molecules approach a solid surface they can be attracted and maintained on the surface in two modes: (1) physisorption and (2) chemisorption.

Physisorption or physical adsorption is a weak bonding due to the induced dipole moment of a nonpolar adsorbate interacting with its own image charge in the polarizable solid, i.e. Van der Waals force. During this process the electronic state of the atom or molecule barely changes. Chemisorption or chemical adsorption is a strong bonding between a gas adsorbate and solid surface, i.e. ionic bonding or covalent bonding. This process involves the electronic structure change of the gas atom or molecule.

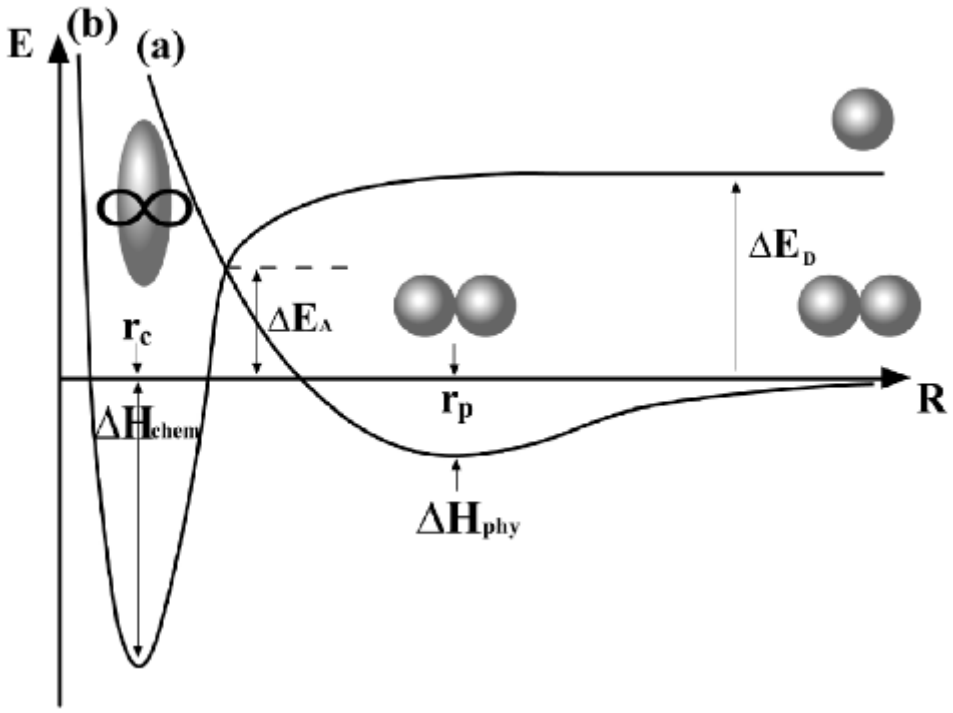

Figure 11: The energy of the system as a function of adsorbate/adsorbent distance (a) physical adsorption and (b) chemical adsorption [89].

According to the Lennard-Jones model, the energy of the system is illustrated as a function of distance between gas atom or molecule and solid surface as shown in Figure 11 [89]. When the distance between the molecule and surface is infinite, the energy of the system is defined as zero. As the molecule approaches the surface it can polarize and induce an equivalent dipole in the solid. Due to the dipole-dipole

interaction, the energy of the system decreases. When the distance between the molecule and the surface decreases to r_p, the Van der Waals force will be balanced by the repulsive force between the atom and substrate. By further approaching repulsion will dominate which will lead to an increase of the system energy. Therefore, at equilibrium distance r_p the system has the lowest energy. The physisorbed molecule is stable there and has the binding energy ΔH_{PHY} with the surface which is typically 10~100 meV. From the distance dependent energy curve for physisorption (curve a) it should be noticed that no activation energy is needed for such a process which means that physisorption is temperature independent. By contrast for desorption an activation energy ΔH_{PHY} is needed. Hence, the physisorption rate can be expressed as,

$$\frac{d\Gamma_{PHY}}{dt} = k_a P\left(\Gamma^O - \Gamma\right) - k_d \Gamma \exp\left(-\frac{\Delta H_{PHY}}{RT}\right) \qquad (6)$$

Where, Γ^O is the density of surface adsorption sites, Γ is the density of surface sites covered by adsorbate, P is gas pressure, k_a is adsorption rate constant., k_d is desorption rate constant, R is gas constant, T is temperature. At steady state, the adsorption rate equals desorption rate i.e. physisorption rate equals zero. By defining $\theta = \frac{\Gamma^O}{\Gamma}$, the fractional coverage, equation 1 yields,

$$\theta = \frac{P}{P + \frac{k_d}{k_a}\exp\left(-\frac{\Delta H_{PHY}}{RT}\right)} \qquad (7)$$

At low gas pressure, equation 7 can be reduced to,

$$\theta \cong \frac{k_a}{k_d}\exp\left(\frac{\Delta H_{PHY}}{RT}\right)P \qquad (8)$$

This equation indicates that fractional coverage has a linear relationship with gas

pressure at low gas concentration and decreases with a temperature increase which means that at high temperature physisorption is negligible.

Besides physisorption, the gas molecules can bond to the solid surface in another mode, chemisorption. The process (curve b) starts from the dissociation of molecules into atoms which needs a dissociation energy ΔE_D. As the atom approaches the surface to certain distance, r_c, a strong chemical bond will form by electron transfer or sharing. In this case a binding energy or heat of chemisorption, ΔH_{CHEM}, is large, typically 1-10 eV. Due to a large dissociation energy, chemisorption generally does not happen directly. In practice, it usually follows physisorption which needs a much smaller amount of activation energy ΔE_a. Hence, the chemisorption rate can be expressed as:

$$\frac{d\Gamma_{CHEMY}}{dt} = k_a P\left(\Gamma^O - \Gamma\right)\exp\left(-\frac{\Delta E_a}{RT}\right) - k_d \Gamma \exp\left(-\frac{\Delta H_{CHEM} + \Delta E_a}{RT}\right) \qquad (9)$$

Therefore, at steady state the equilibrium fractional coverage can be written as,

$$\theta = \frac{k_a}{k_d}\exp\left(\frac{\Delta H_{CHEM}}{RT}\right) \qquad (10)$$

It's easy to understand from equation 9 that both adsorption and desorption process require activation energy. So chemisorption occurs at higher temperatures than physisorption.

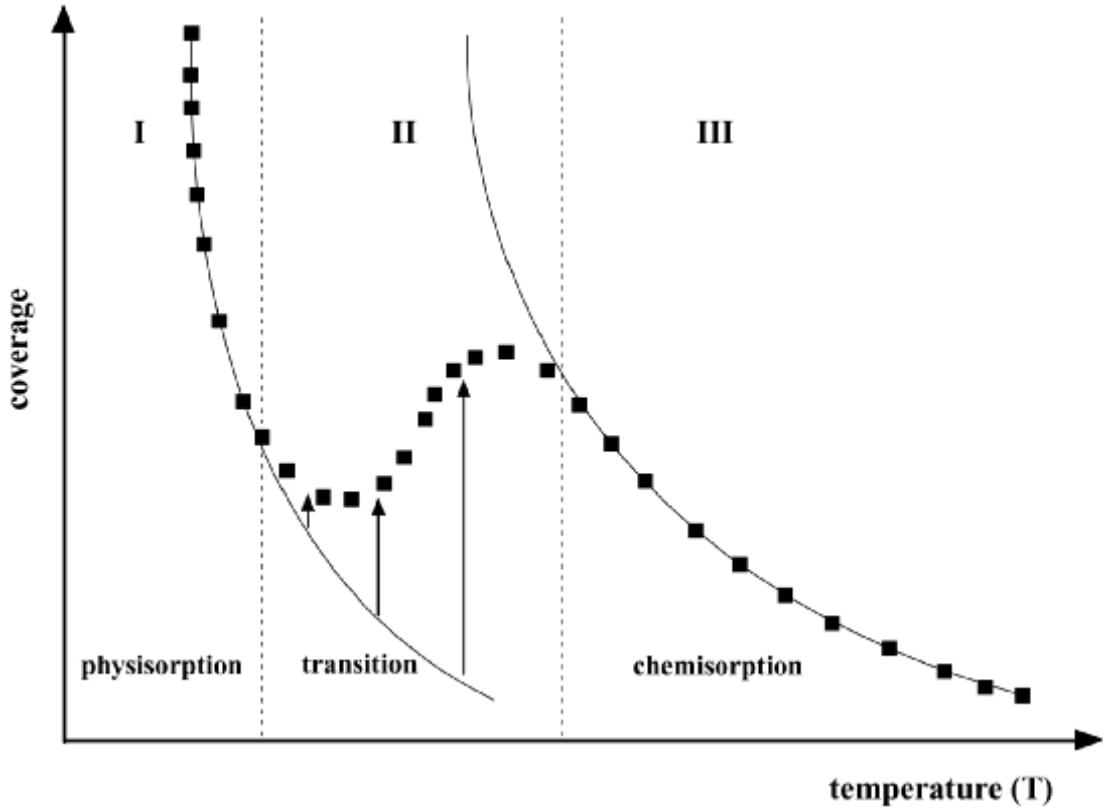

Figure 12: Typical temperature dependence of adsorption coverage [89].

The typical temperature dependence of adsorption coverage is sketched as a dotted curve in Figure 12. At low temperature (region I), the thermal energy is not enough to overcome the activation energy, ΔE_a, so only physisorption occurs. The equilibrium coverage follows the physisorption curve which can be expressed as equation 3. At high temperatures (region III), enough thermal energy is provided to activate both adsorption and desorption processes of chemisorption. Therefore, equilibrium coverage can be reached and the chemisorption curve is followed which is given by equation 5. In the intermediate temperature range (region II), on one hand thermal energy is enough to activate the adsorption process of chemisorption. So chemisorption sets in and transition from physisorption to chemisorption starts. On the other hand, the thermal energy is not enough to activate the desorption process of chemisorption. Therefore, equilibrium coverage of chemisorption can't be reached.

Then, a question arises: how can the adsorption be balanced otherwise it never stops? Actually, it can be explained by the activation energy ΔE_a. In practice, ΔE_a is not constant, it increases with the coverage. The solid surface is heterogeneous. So adsorbate will first fill the site with lowest energy i.e. highest ΔH_{CHEM}. As a result, ΔH_{CHEM} decreases with increasing coverage. In the Lennard-Jones model, this is expressed as the upward shift of curve b in Figure 4. As curve a is not affected, ΔE_a will increase as a result. When the thermal energy is not enough to overcome the increased ΔE_a chemisorption stops. Hence, if the temperature increases again, the adsorption will continue which explains the increasing coverage with temperature in region II. It should be noticed that such chemisorption is irreversible due to the lack of chemical desorption. So only lowering the temperature or pressure will result in residual coverage. Therefore, metal oxide semiconductor sensors operated in intermediate temperature range require high temperature surface cleaning. Otherwise, the sensor will inevitably become less sensitive due to the reduction of active sensing sites.

2.2.2. Theory of adsorption and tin oxide sensor sensing mechanism

It is easy to understand that the electron energy level of an atom in vacuum is different from the one in a material. At the surface which can be recognized as a defect of materials, electronic band structure will change from the bulk material to the vacuum. Thus, new electronic surface states are formed at atom layers which are closest to the surface. For ionic materials, the unoccupied orbital on the cation acts as an acceptor-like surface state (Lewis acid site) and the occupied orbital on the anion acts as a donor-like state (Lewis base site). For a covalent material, atoms at the

surface form dangling bonds. Besides the intrinsic surface state which is only due to termination of lattice periodicity another surface state, so called extrinsic surface state originates from the adsorption of gas impurities. When a foreign atom or molecule is adsorbed on the surface, electrons can either transfer from bulk material to foreign species if the induced surface state is lower than the Fermi level of the solid (average energy level of electrons), or from foreign species to bulk material if the induced surface state is higher than the Fermi level of the solid. Thus, foreign species are chemisorbed and cause an electric field due to the surface charge layer formed. This electrostatic field will bend the energy band of the solid. A negative surface charge layer will bend the bands upward while a positive surface charge layer will bend the bands downward as shown in Figure 13. As the Fermi level is pushed back to the band gap, the charge carrier concentration of semiconductors is reduced and a depletion region is formed which compensates for the surface charge layer.

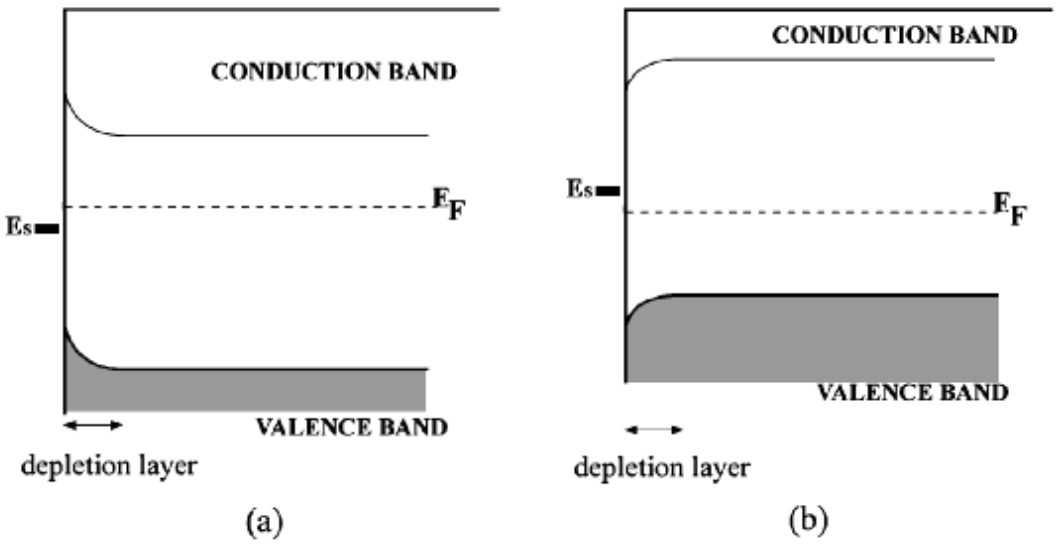

Figure 13: Band bending in the near surface region of (a) an n-type semiconductor (b) a p-type semiconductor; ES, surface state energy level

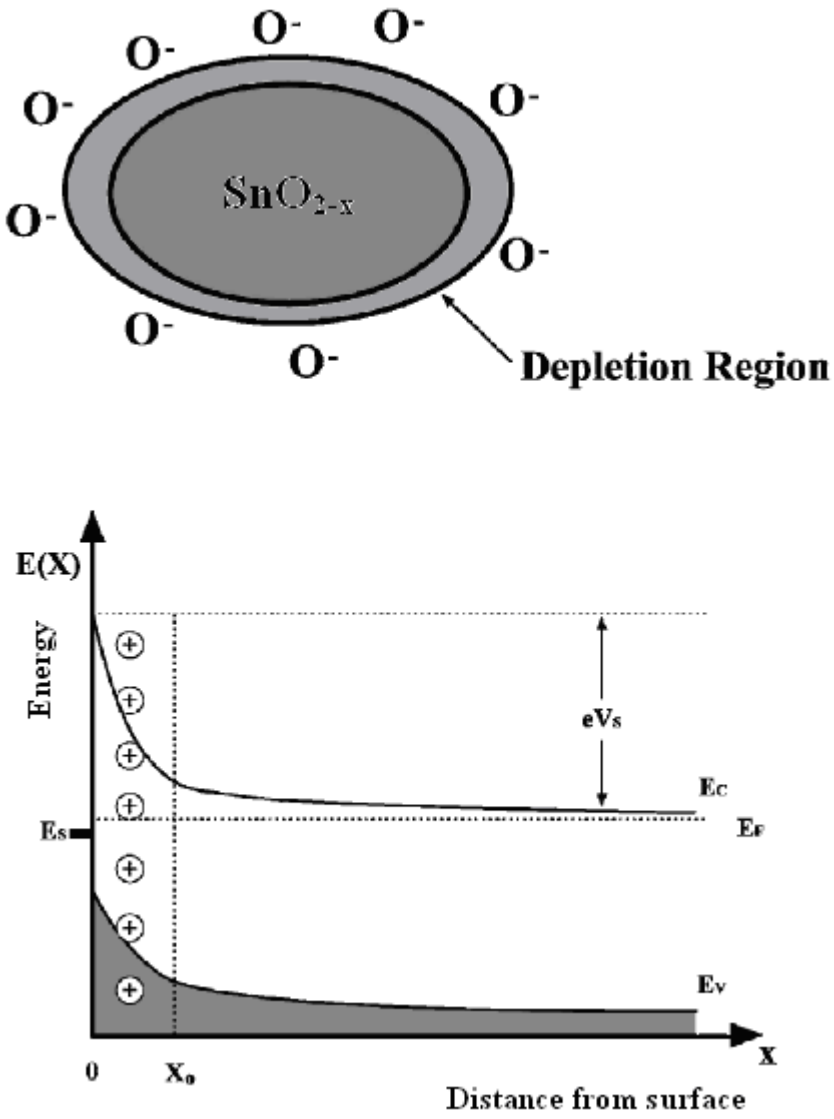

Figure 14: Depletion layer formed at the surface of tin oxide

Taking tin oxide solid and oxygen gas as the example which is illustrated in Figure 14, electrons flow due to the electron energy level difference between the oxygen induced surface state and the tin oxide bulk material. Oxygen captures electrons and forms a negative surface charge layer on the surface. A depletion layer within x_0 from the surface is formed and the electronic bands bend upward. The charge distribution can be quantitatively derived from the one dimensional Poisson's equation [90]:

$$\frac{d^2V}{dx^2} = -\frac{\rho(x)}{\varepsilon_0 \varepsilon_r} \qquad (11)$$

where V is the potential, x is the distance from surface, ε_0 is the permittivity of vacuum, ε_r is the relative permittivity of the semiconductor, ρ is the net charge density which consists of electrons (n) , holes (p), ionized donor (N_D^+) and ionized acceptor (N_A^-). In the depletion region, the concentration of electrons and holes is assumed to be zero. Thus, the net charge density within the distance x_0 can be expressed as:

$$\rho = e\left(N_D^+ - N_A^-\right) \qquad (12)$$

Substituting equation (12) into equation (11) and integrating once,

$$E(x) = \frac{dV}{dx} = -\frac{e\left(N_D^+ - N_A^-\right)}{\varepsilon_0 \varepsilon_r} x + cons. \qquad (13)$$

Assuming the potential in the depletion region smoothly changes into the potential of the bulk material V_b one can get the boundary condition that $V = V_b$, $\frac{dV}{dx} = 0$, at $x = x_0$. Thus, equation (13) becomes,

$$E(x) = \frac{dV}{dx} = -\frac{e\left(N_D^+ - N_A^-\right)}{\varepsilon_0 \varepsilon_r}(x - x_0) \qquad (14)$$

Integrating equation (14) and given the boundary one can obtain,

$$V(x) = -\frac{e\left(N_D^+ - N_A^-\right)}{2\varepsilon_0 \varepsilon_r}(x - x_0)^2 + V_b \qquad (15)$$

According to the calculation above, functions of the space charge, electric field, and potential energy can be illustrated as in Figure 15.

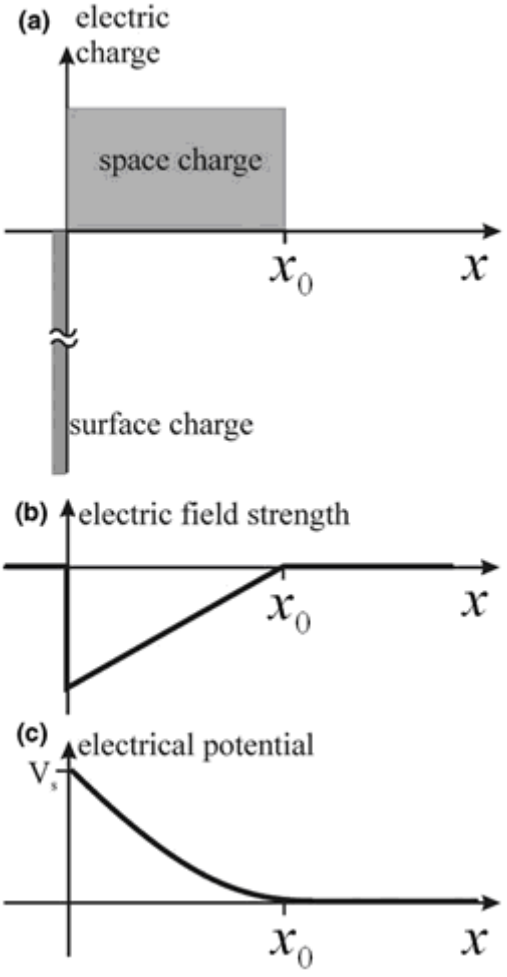

Figure 15: Functions of physical properties (a) the space charge, (b) the electric field, and (c) the potential [90].

By defining $V_b = 0$, surface barrier height, V_S, at $x = 0$ becomes,

$$V_S = \frac{e\left(N_D^+ - N_A^-\right)}{2\varepsilon_0\varepsilon_r} x_0^{\,2} \qquad (16)$$

Thus, the energy barrier, eV_S, which electrons must overcome to move to surface states becomes,

$$eV_S = \frac{e^2\left(N_D^+ - N_A^-\right)}{2\varepsilon_0\varepsilon_r} x_0^{\,2} \qquad (17)$$

Based on charge neutrality, surface charge should equal space charge i.e.

$$N_S = \left(N_D^+ - N_A^-\right)x_0 \qquad (18)$$

where N_S is the number of occupied surface states per unit area. Substituting equation (18) into equation (17) and eliminating x_0, one can obtain,

$$eV_S = \frac{e^2 N_S^2}{2\varepsilon_0 \varepsilon_r \left(N_D^+ - N_A^-\right)} \qquad (19)$$

It is easy to see that the activation barrier is proportional to the square of surface coverage (N_S) and increases with increasing coverage. For an n-type semiconductor $N_D^+ >> N_A^-$, so the surface coverage can be expressed as,

$$N_S = \left(\frac{2\varepsilon_0 \varepsilon_r N_D^+ V_S}{e}\right)^{\frac{1}{2}} \qquad (20)$$

Based on equation (20) and assuming a reasonable impurity concentration (10^{25}/m^3), a fairly high barrier potential (1V) and a total number of surface sites (10^{19}/m^2), Weisz [91] calculated the fractional coverage θ and obtained the value 0.9%. Given the high sensitivity of such kind of sensor, the surface barrier at intergranular contact is believed to play a key role.

By comparing the neck width and Debye length of electron L_D which can be expressed as equation (21), the intergranular contacts can be classified into three kinds: (1) Open neck (2) Closed neck and (3) Schottky contact.

$$L_D = \left(\frac{\varepsilon_0 \varepsilon_r kT}{e^2 n_b}\right)^{\frac{1}{2}} \qquad (21)$$

where k is the Boltzmann constant, n_b is the electron density of bulk material.

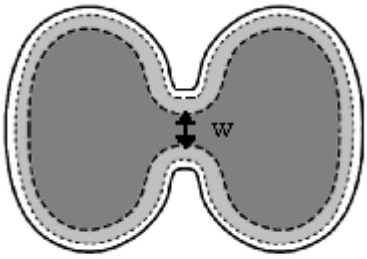

Figure 16: Open neck

When the neck width is larger than $2L_D$ the contact is called open neck as shown in Figure 16. The highly resistive depletion layer is parallel connected with the lower resistive bulk grain at the neck. Hence, the conductance is governed by the undepleted layer width w and can be expressed as:

$$G \propto w \exp\left(-\frac{\Delta E_b}{kT}\right) \qquad (22)$$

where ΔE_b is the activation energy of electron from donor level to conduction band in bulk material. This case is often found in well sintered ceramics.

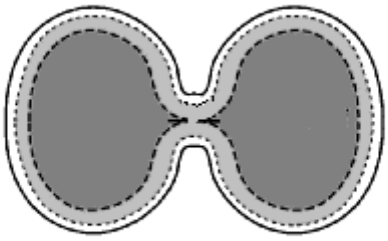

Figure 17: Closed neck

When the neck width is smaller than $2L_D$, the contact is called closed neck as shown in Figure 17. The depletion layers at opposite surfaces at the neck overlap and

form a more resistive contact. The conductance is dominated by the activation of electron from surface state to conduction band at the surface and can be written as:

$$G \propto \exp\left(-\frac{\Delta E_S}{kT}\right) \qquad (23)$$

where ΔE_S is activation energy of electron from surface state to conduction band at the neck. This case usually can be found in less sintered ceramics.

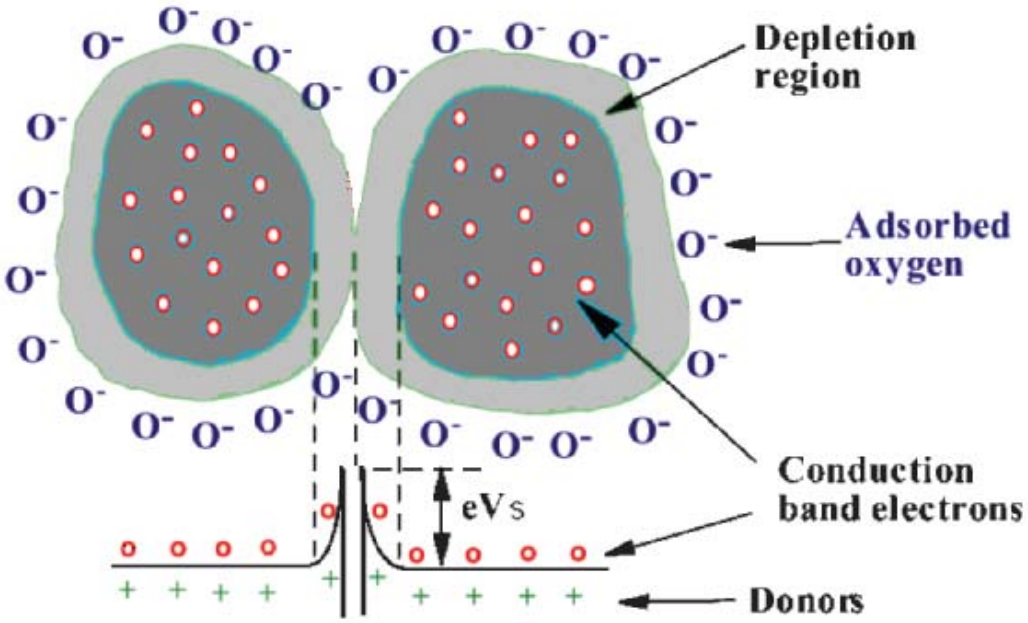

Figure 18: Schottky contact

When no neck exists and two particles with diameter greater than 2 L_D are only "pressed" together, the contact is called Schottky contact as shown in Figure 18. Electrons must overcome the energy barrier eV_S which appears in equation (19). Thus, the conductance can be expressed as:

$$G \propto \exp\left(-\frac{eV_S}{kT}\right) \qquad (24)$$

In practice a sensor usually consists of all three types of contact. At high

sintering temperature Schottky contact can convert to neck type contact. Thus, thermal treatment of the sensing element will affect the composition of different contacts which determines the response characteristics of a sensor. To describe the response of the tin oxide sensor various empirical formulas have been proposed as shown in table 2.

Table 2: Different formulas describing response of semiconductor gas sensor.

Reference	Formula
[92]	$R = R_0(1 + KC)^{\alpha}$
[93]	$R = R_0 KC^{\alpha}$
[94]	$R = \alpha \log C + \beta$
[95]	$G = KC^{\alpha}$
[96]	$G_0 - G = GC^{\alpha}$
[97]	$G = G_0 \exp(KC^{\alpha})$
[98]	$G = G_0 + KC^{\alpha}$

G: conductance in gas; G_0: conductance in air; R: resistance in gas; R_0: resistance in air; C: gas concentration; K, α , β : constants.

CHAPTER 3: OBJECTIVES OF RESEARCH

The final goal of the research project is to establish a remote monitoring system for plant health. The objective of this research is to identify the capability of tin oxide semiconductor sensor to detect Methyl Jasmonate, an important chemical vapor related to a plants' natural defense system. By studying the concentration dependence, temperature dependence, humidity dependence, recovery time, stability of the sensor, the suitability of a semiconductor type sensor for detection of insect infestation will be determined.

CHAPTER 4: EXPERIMENTAL PROCEDURE

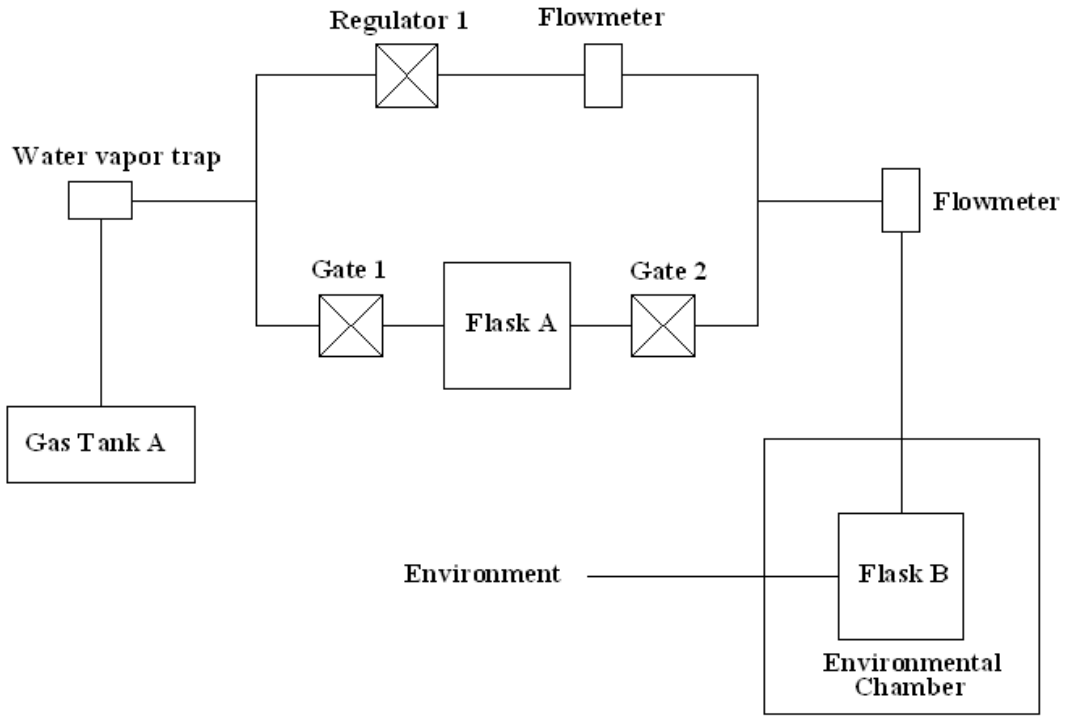

Figure 19: Schematic of gas flow circuit for concentration dependence and temperature dependence tests.

The gas flow circuit for concentration dependence and temperature dependence tests is presented in Figure 19. A compressed air tank furnished by Airgas, Inc was used as the carrier gas supply. A water vapor trap was installed to remove any moisture in the gas supply. Gas flow rate was monitored by a Mass flow meter (FMA1700/1800) made by OMEGA Engineering, Inc. Two TGS 2620 tin oxide sensors manufactured by Figaro, Inc were put in the flask B for detection tests. In

addition, a thermocouple and a battery-powered remote temperature and humidity logger (USB 502) are located in flask B to monitor the ambient temperature and the humidity. The flask B is kept in an environmental chamber (ECT-3) manufactured by ESPEC North America, Inc to control the temperature. TGS 2620 (Figure 20) is a thick film type semiconductor sensor with an alumina substrate. It is highly sensitive to the vapors of organic solvents as well as other volatile vapors. The sensing element is integrated with a heater to raise the temperature to about 400°C. Pins 1 and 4 are connected to a DC power supply (Agilent E3611A) for heating. Pins 2 and 3 are connected to a data acquisition system (Agilent 34970A) for resistance response measurements.

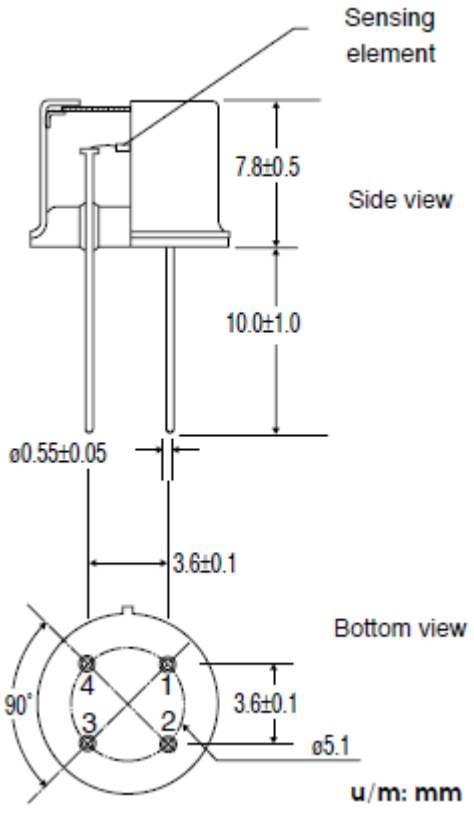

Figure 20 Schematic of TGS 2620 tin oxide sensor.

4.1. Concentration Dependence Test

For the concentration dependence test the total gas flow rate was fixed at 0.2L/min. Before the tests, the sensors were kept in air in an environmental chamber for 7 days for conditioning. To establish the base line of the signal, regulator 1 was open; gates 1 and 2 were closed. When the resistances of the sensors were stable regulator 1 and gates 1 and 2 were opened. Thus, carrier air gas will flow into the liquid Methyl Jasmonate which was kept in flask A and take the chemical vapor into the testing chamber (flask B). The sensors were exposed to the chemical vapor for 30 minutes. Then gates 1 and 2 were closed for recovery test. When the resistances of the sensors recover and became stable again another test cycle was started. To change the concentration of the target gas vapor, the gas flow rate through flask A and through the bypass (regulator 1) were regulated by gas flow regulator 1. The partial flow rate through flask A was set at 8 different points (0.02 L/min, 0.04 L/min, 0.06 L/min, 0.08 L/min, 0.10 L/min, 0.12 L/min, 0.16 L/min, 0.20 L/min) but the total flow rate was kept a constant at 0.2L/min. The temperature is maintained at 25°C by the environmental chamber and monitored by thermocouple.

To determine the actual concentration of Methyl Jasmonate at different flow rates Gas Chromatography (GC) was used. A Varian CP-3380 GC machine with DB-5 column and flame ionization detector (FID) was used for this study. To make standard solutions different amounts of Methyl Jasmonate (0.1μL , 0.5μL, 1μL, 5μL, 10μL, 100μL) was dissolved in 5mL Dichloromethane. Gas samples at different flow rates were collected using a volatile collection trap (VCT - 1/4 - 3 - HSQ-P), which was fabricated by ARS, Inc. The volatile collection trap was connected to the gas flow tube for three hours. Then 2mL Dichloromethane was injected into the trap to extract the Methyl Jasmonate adsorbed. Every time 0.1μL of standard solutions or gas sample

solutions was injected into the GC for test using a micro syringe. During the experiment the injector of the GC was set at 275°C and the FID was set at 320°C. The column was initially set at 45°C for 5 minutes and then heated up to 300°C at the rate of 15°C/min. The hydrogen pressure for the column was fixed at 40 psi, the air pressure was 60 psi and the carrier gas helium was 80 psi.

4.2. Temperature Dependence Test

For the temperature dependence test the gas flow rate was kept constant at 0.2L/min. Before the tests the sensors were kept in air in the environmental chamber for 7 days for conditioning. At the beginning regulator 1 was opened; gates 1 and 2 were closed to establish a baseline. When the resistances of the sensors were stable regulator 1 was closed and gates 1 and 2 were opened in order to expose the sensors to chemical vapor for 30 minutes. Then regulator 1 was opened, gates 1 and 2 were closed for the recovery test. When the resistances of the sensors recovered, the temperature was changed by the environmental chamber. Consequently, the resistances of the sensors changed. When the sensor outputs were stable again, another response and recovery test cycle was performed. Test cycles were performed at 9 different ambient temperatures (-22°C, -12°C, -2°C, 7°C, 17°C, 22°C, 27°C, 32°C, 37°C). During the test the temperature was monitored by thermocouple.

4.3. Humidity Dependence Test

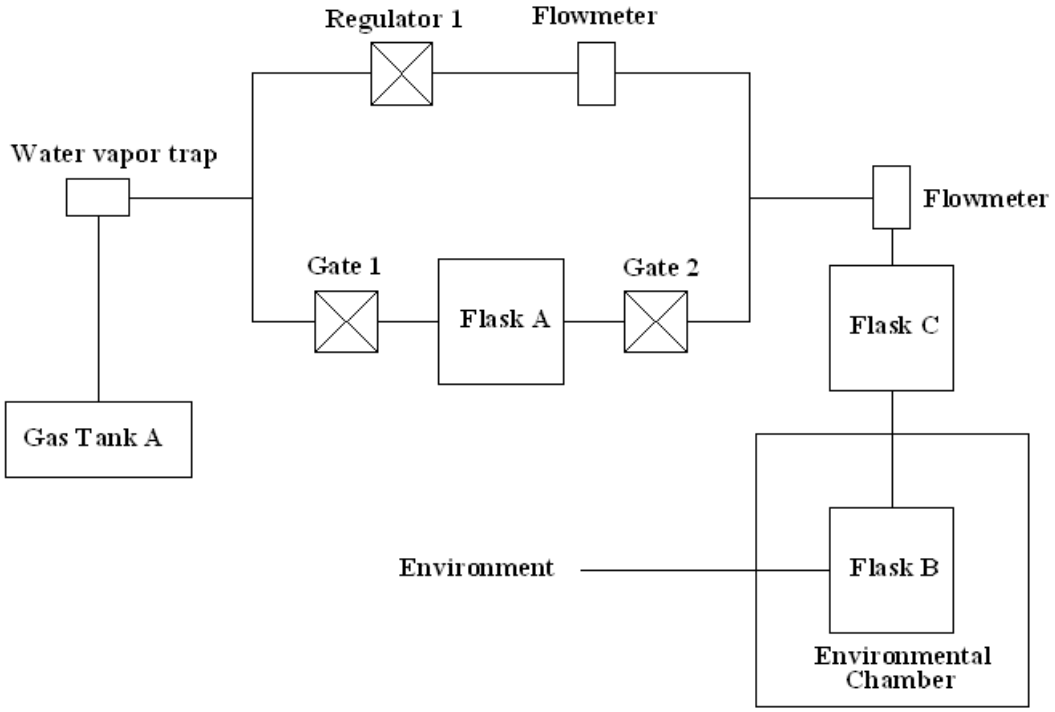

Figure 21: Schematic of gas flow circuit for humidity dependence tests.

Figure 21 illustrates the gas flow circuit for humidity dependence tests. Flask C with saturated salt solution was added to provide constant moisture. For humidity dependence tests the total gas flow rate was fixed at 0.2L/min. Before the tests the sensors were kept in air in the environmental chamber for 7 days for conditioning. To establish the base line of the signal, regulator 1 was open; gates 1 and 2 were closed. When the resistances of the sensors were stable regulator 1 was closed and gates 1 and 2 were opened. The sensors are exposed to the chemical vapor for 30 minutes. Then regulator 1 was opened and gates 1 and 2 were closed for the recovery test. When the resistances of the sensors recovered, the humidity was changed by alternating the kind of saturated salt solution in Flask C. Consequently, the resistances of the sensors changed. When they were stable again, another response and recovery test cycle was performed. The humidity was monitored by the humidity sensor.

CHAPTER 5: RESULTS AND DISCUSSION

5.1. Concentration dependence study

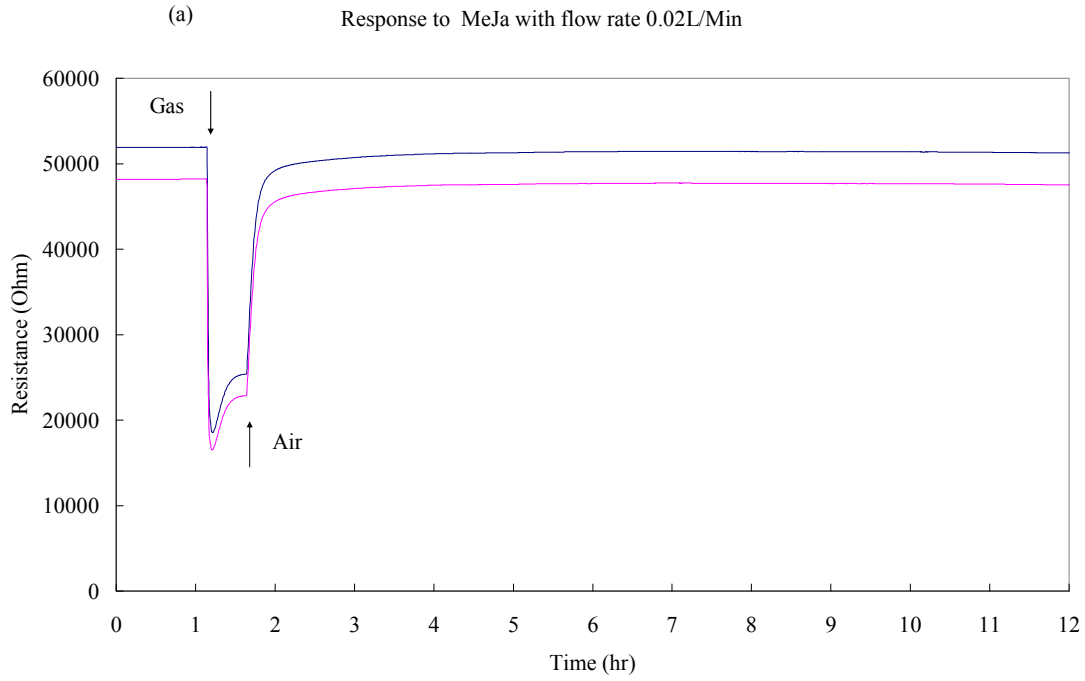

Figure 22a: Sensors' responses to MeJa with partial flow rate 0.02L/Min.

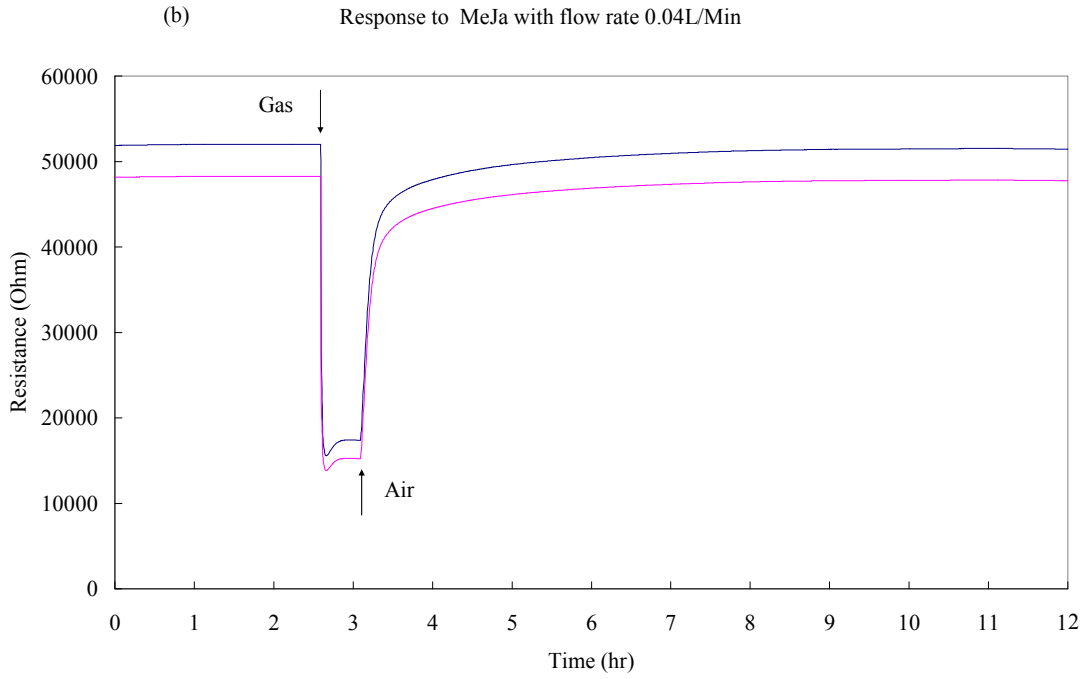

Figure 22b: Sensors' responses to MeJa with partial flow rate 0.04L/Min.

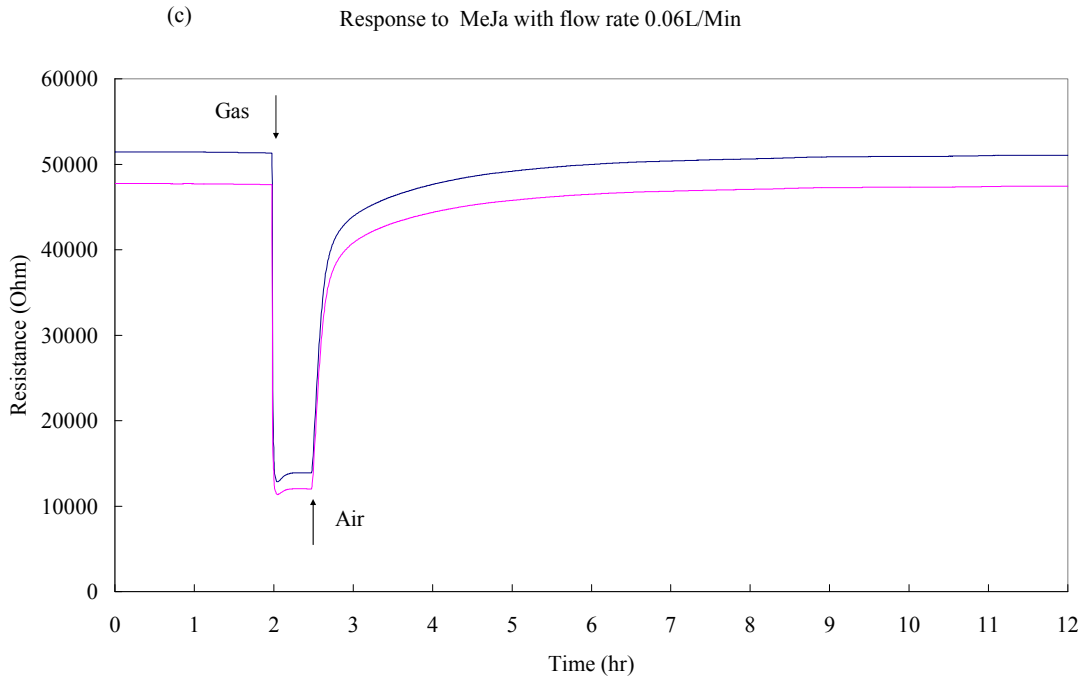

Figure 22c: Sensors' responses to MeJa with partial flow rate 0.06L/Min.

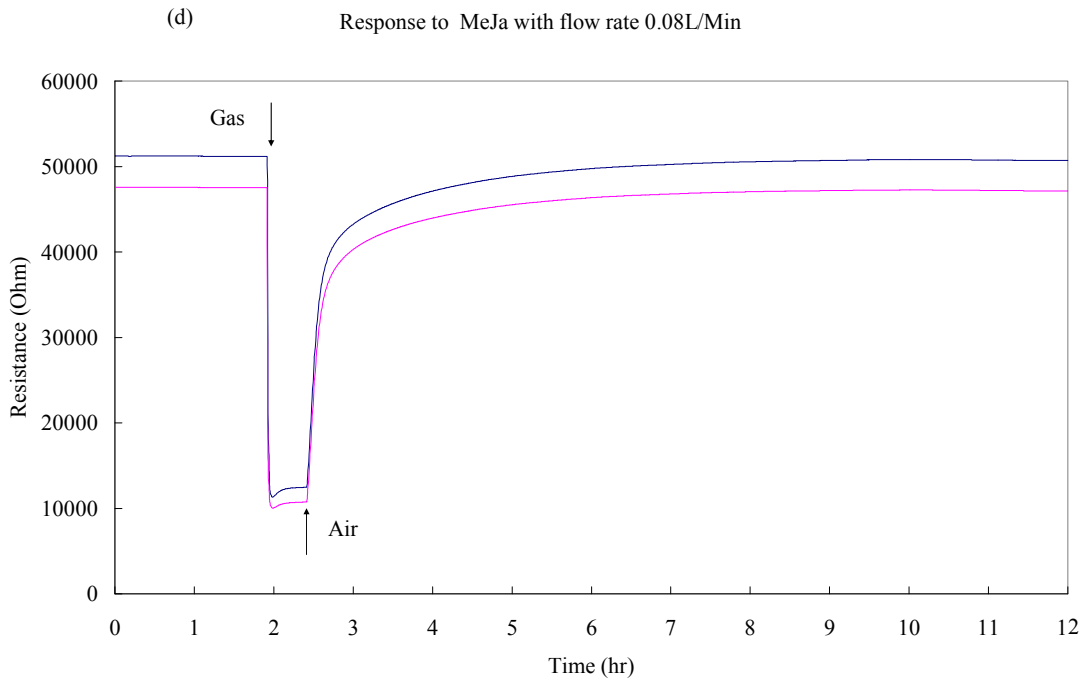

Figure 22d: Sensors' responses to MeJa with partial flow rate 0.08L/Min.

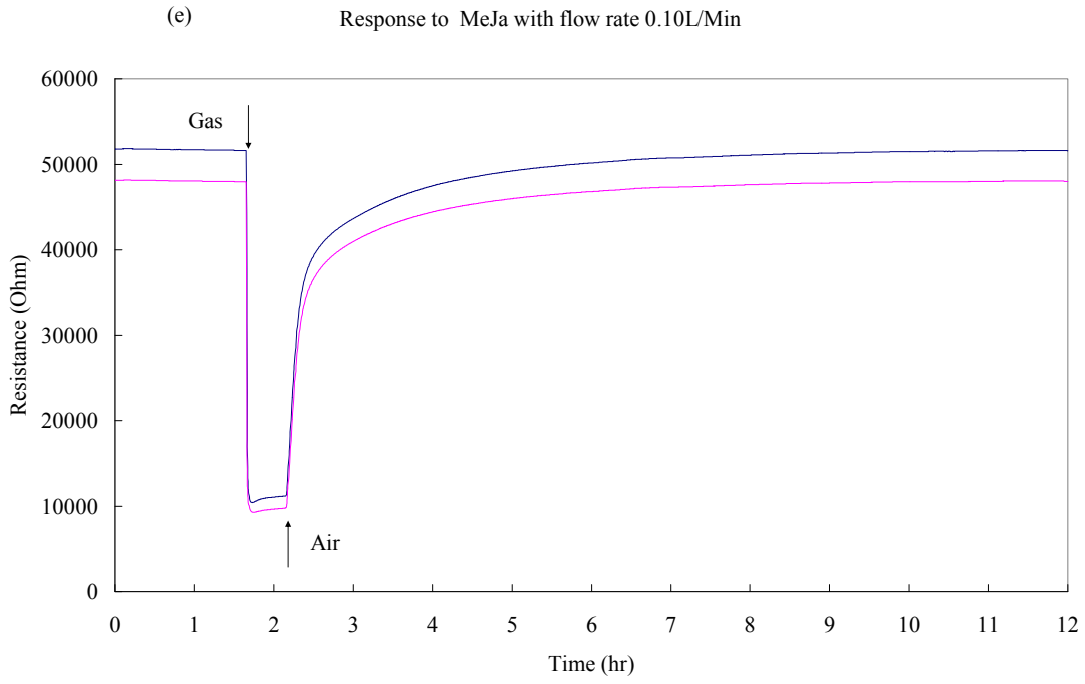

Figure 22e: Sensors' responses to MeJa with partial flow rate 0.10L/Min.

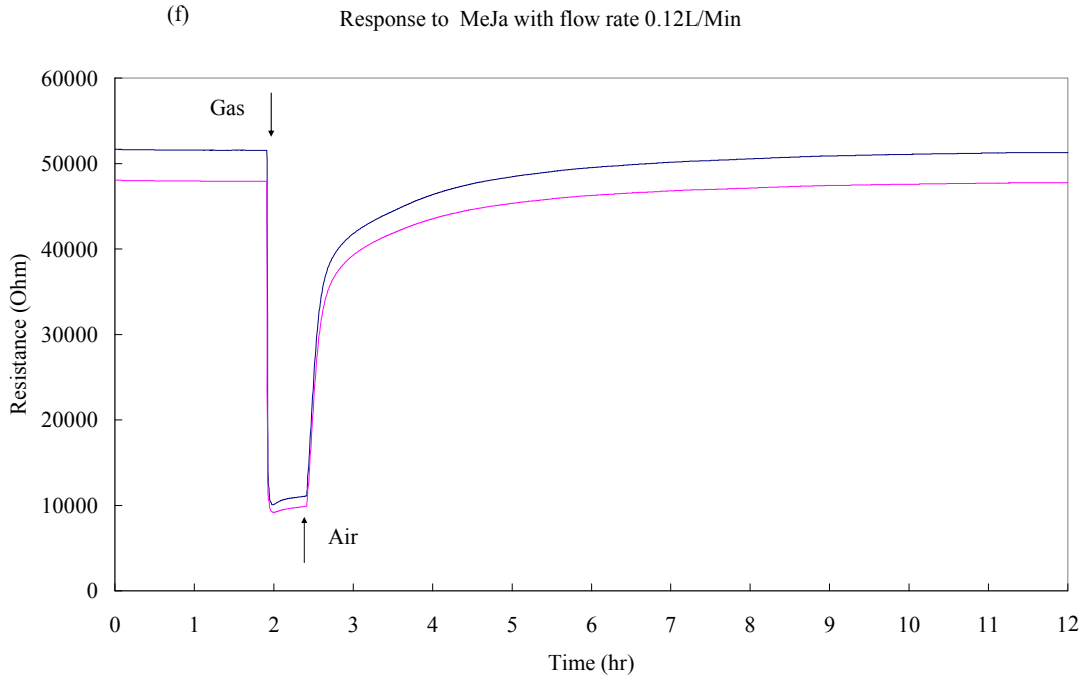

Figure 22f: Sensors' responses to MeJa with partial flow rate 0.12L/Min.

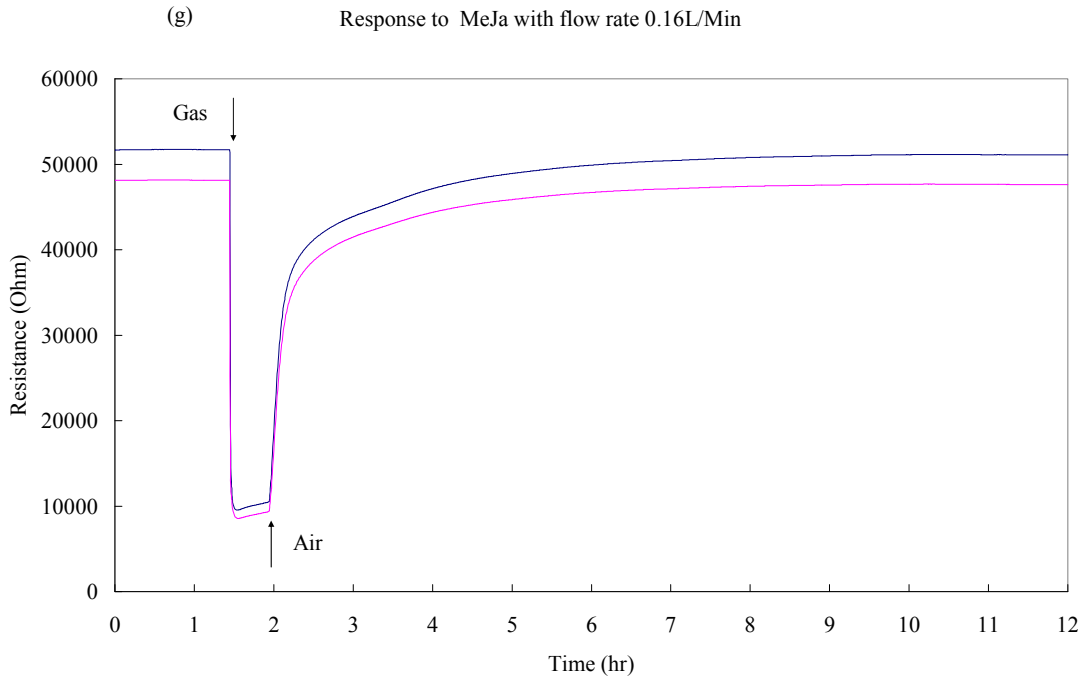

Figure 22g: Sensors' responses to MeJa with partial flow rate 0.16L/Min.

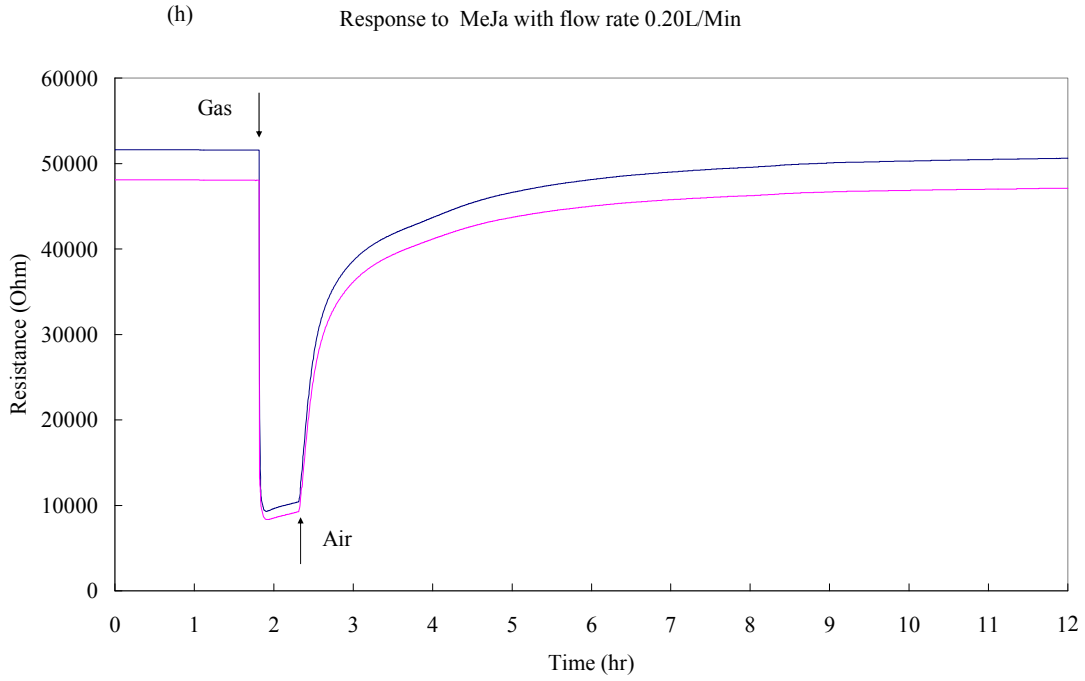

Figure 22h: Sensors' responses to MeJa with partial flow rate 0.20L/Min.

Figure 22a to Figure 22h illustrate the resistances change of the sensors to MeJa at different partial flow rates. When MeJa is introduced, the resistance of the sensor decreases sharply and reaches the lowest value in 4 minutes. Then the resistance gradually increased and became stable again. After being exposed to the chemical vapor for 30 minutes the sensors are exposed to air flow again. The resistance can recover to 80 percent of initial resistance in about 40 minutes and fully recover in about 8 hours. Therefore, the sensors have a good reusability. The flat base lines indicate a good stability of the sensors.

To determine actual concentration of MeJa at different partial flow rates, GC was used. Six standard solutions were made for the tests with different amounts of Methyl Jasmonate (0.1μL, 0.5μL, 1μL, 5μL, 10μL, 100μL), which were dissolved in 5mL Dichloromethane. The results are shown in Figure 23.

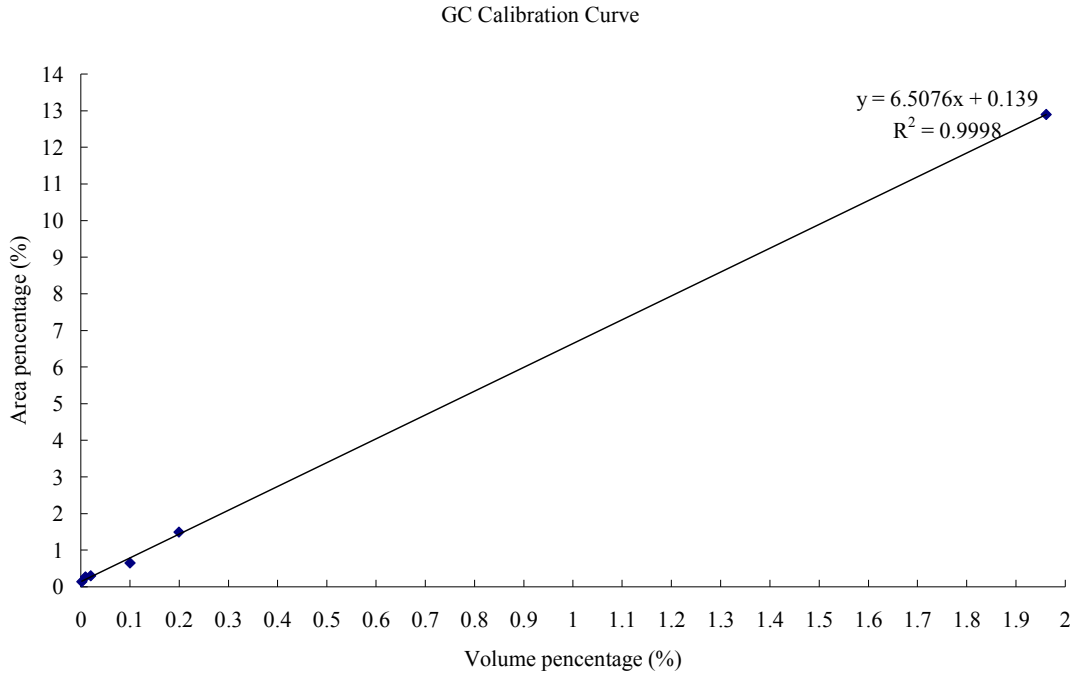

Figure 23: GC calibration curve.

The peak area is proportional to the amount chemicals injected into the GC. The volume percentage of a chemical can be expressed as,

$$V_i\% = \frac{f_i A_i}{\sum f_i A_i} \qquad (25)$$

$V_i\%$ is the volume percentage of a chemical, f_i is the response factor of GC, A_i is the peak area of a chemical. In certain ranges the response factor can be assumed to be the same for similar chemicals. Hence, the volume percentage becomes proportional to the peak area percentage. The high relevance coefficient indicates that the assumption here is safe. Using the calibration curve the concentrations of gas samples were calculated and are shown in table 3.

Table 3: Calculated concentrations of different gas samples

Flow rates of gas samples (L/Min)	Calculated concentration (ppm)
0.02	3.32
0.04	6.58
0.06	9.21
0.08	11.04
0.10	12.84
0.12	14.10
0.16	15.59
0.20	17.46

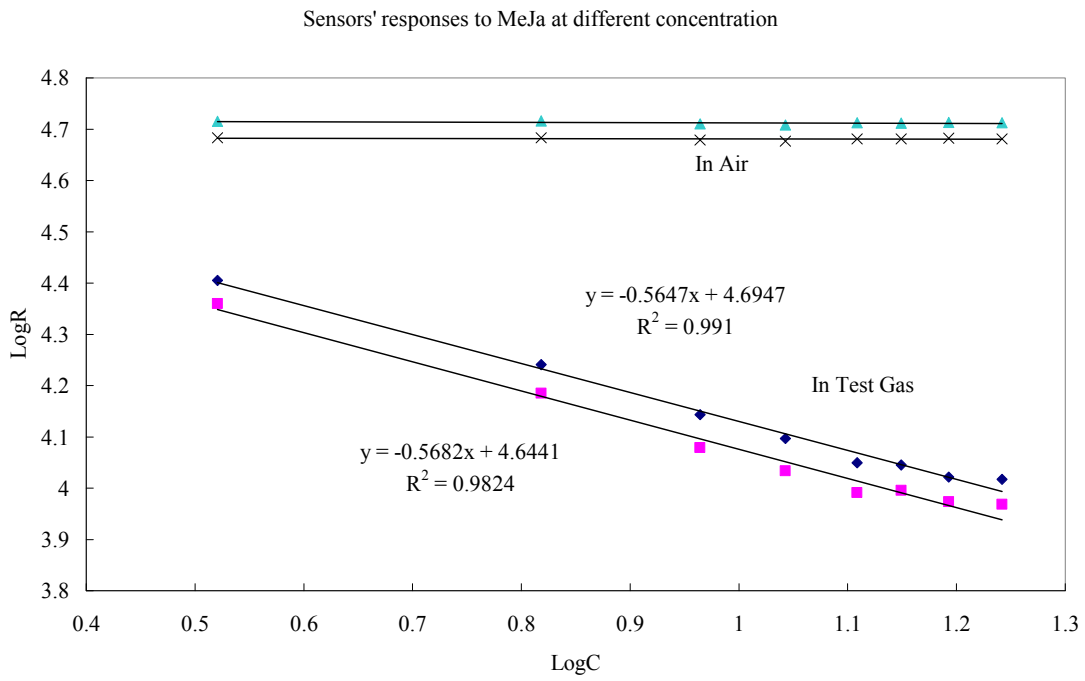

Figure 24: Sensors' responses to MeJa at different concentration.

Using the concentration obtained by GC, the logarithmic resistances of sensors is plotted verses logarithmic concentration as shown in Figure 24. The resistances of the sensors in air R_a are almost constant which indicates a good reusability of the sensors. The resistances of the sensors in test gas R_g decrease with increasing concentration of MeJa and show a linear relationship with concentration on a

logarithmic scale. Therefore, the resistance of the sensor in gas is found to follow the expression (26) which is the well known power law [99].

$$LogR_g = \alpha LogC + \beta \quad \text{or} \quad R_g = KC^n \quad (26)$$

Where C is the concentration of the gas, α, β, K, n are constants.

By defining the relative sensor sensitivity S as,

$$S = \frac{R_a}{R_g} \qquad (27)$$

it is found that the relative sensor sensitivity increases from about 2 to 5 with increasing concentration of MeJa and follows the power law (Figure 25).

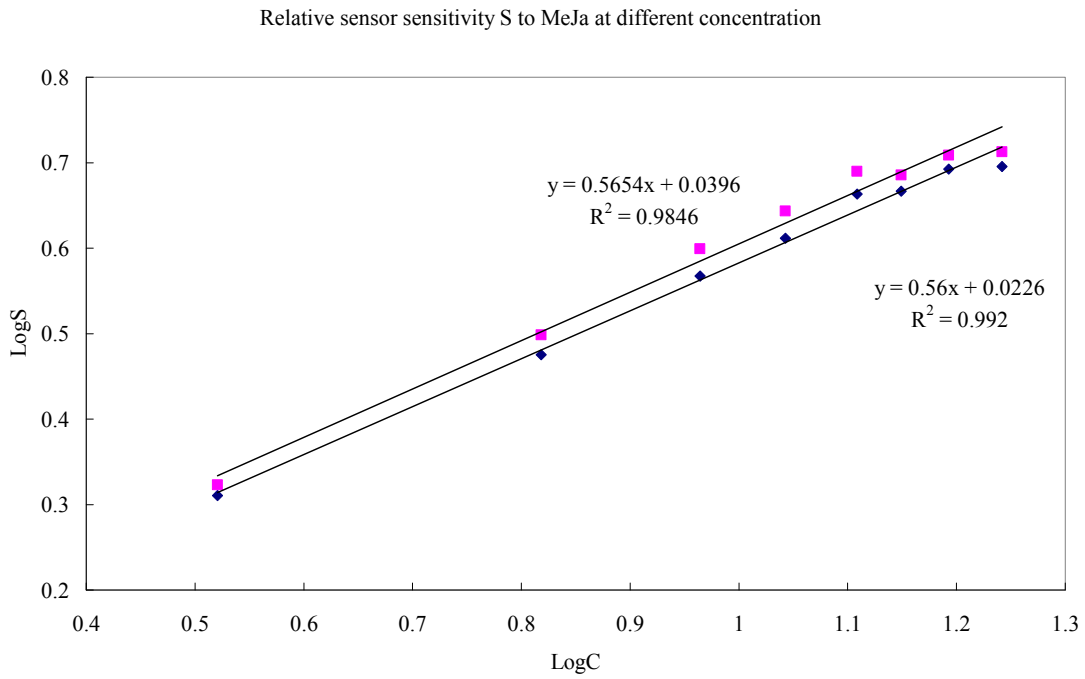

Figure 25: Relative sensor sensitivity S to MeJa at different concentration

5.2. Temperature dependence study

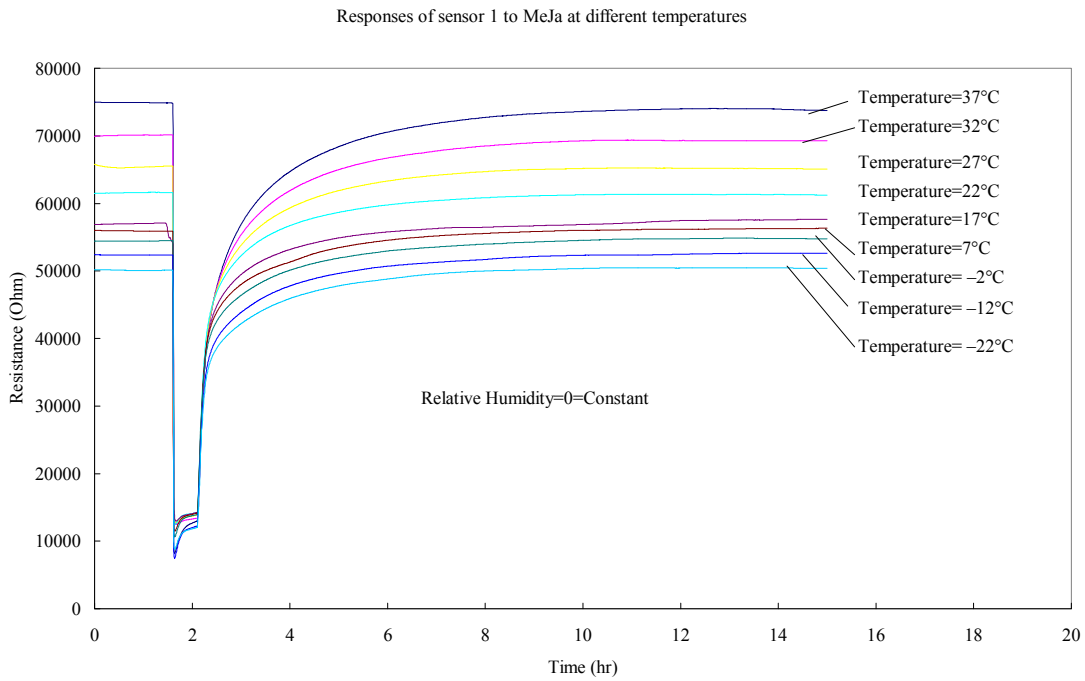

Figure 26a: Responses of sensor 1 to MeJa at different temperatures

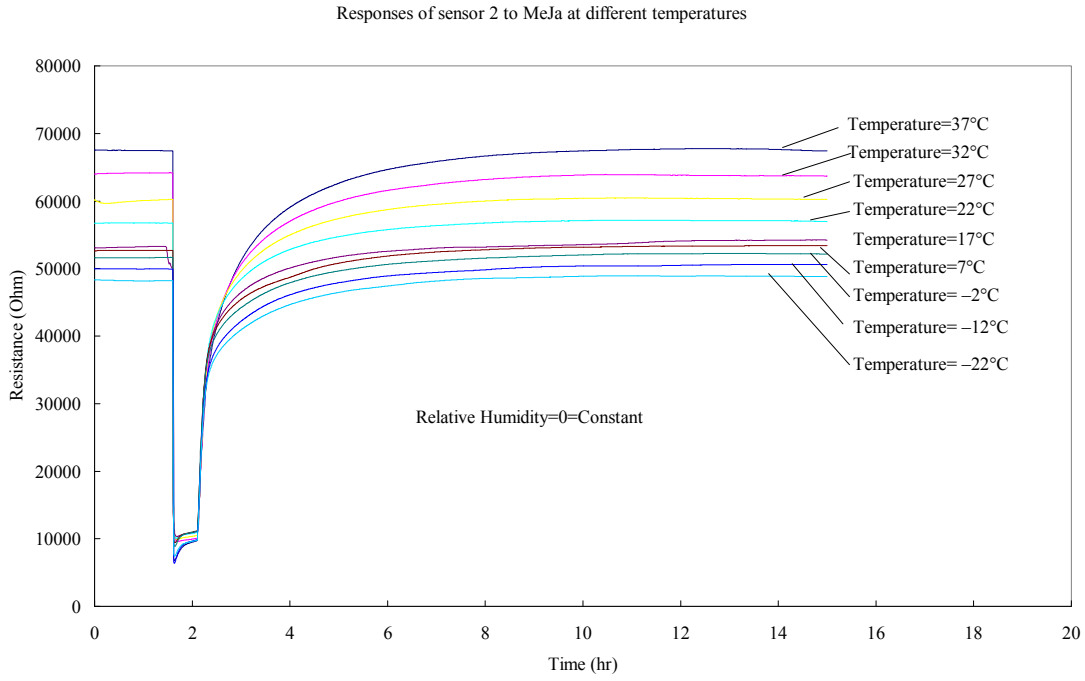

Figure 26b: Responses of sensor 2 to MeJa at different temperatures

Figure 26a and Figure 26b show the responses of two sensors at different temperatures. The flat initial resistances of the sensors and the ability to recover to the initial resistances indicate good stability and reusability at different temperatures. With increasing ambient temperature, the sensor resistances in air solely decrease, and the sensor resistances in test gas first increase then decrease as shown in Figure 27.

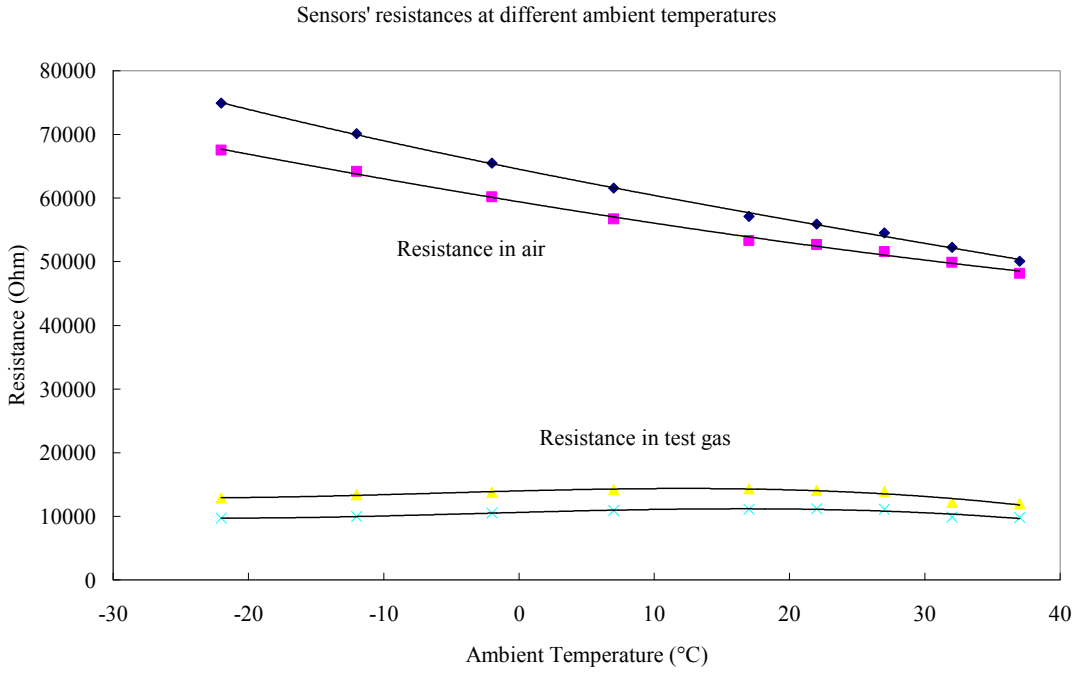

Figure 27: Sensors' resistances at different ambient temperatures.

Hence, the sensors have relatively low relative sensitivity S at around 20°C about 4 to 5, and S decreases with increasing temperature (Figure 28).

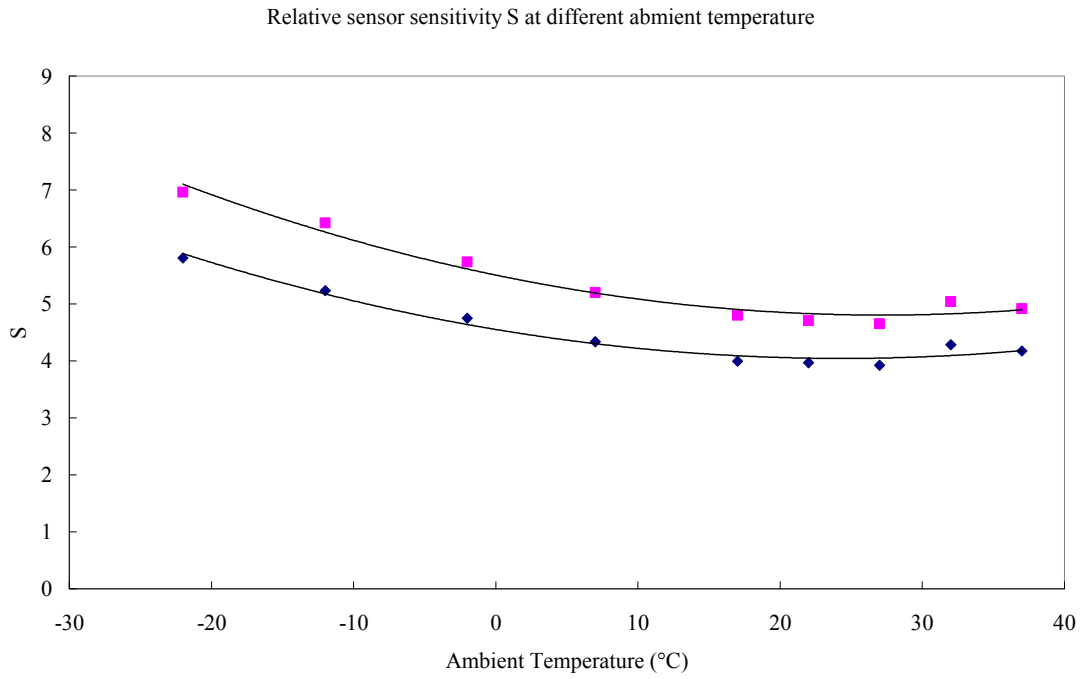

Figure 28: Relative sensor sensitivity S at different ambient temperatures.

According to the report of Figaro Inc, the TGS 2620 sensor is heated by an integrated heater whose working voltage and current is 5V and 42mA respectively. Thus, the working temperature of the sensing element is elevated to about 400°C when the sensor is working at the ambient temperature of 20°C. For practical in field use, the sensor probably will work in the temperature range from -30°C to 40°C. Hence, the sensor is tested at different temperatures within that range. Jian-wei et al reports that the ambient temperature has a linear superposition effect on sensor's working temperature as shown in Figure 29 [100]. Hence, during the temperature dependence test, the temperature of the sensing element is estimated to be in the range from 350°C to 420°C.

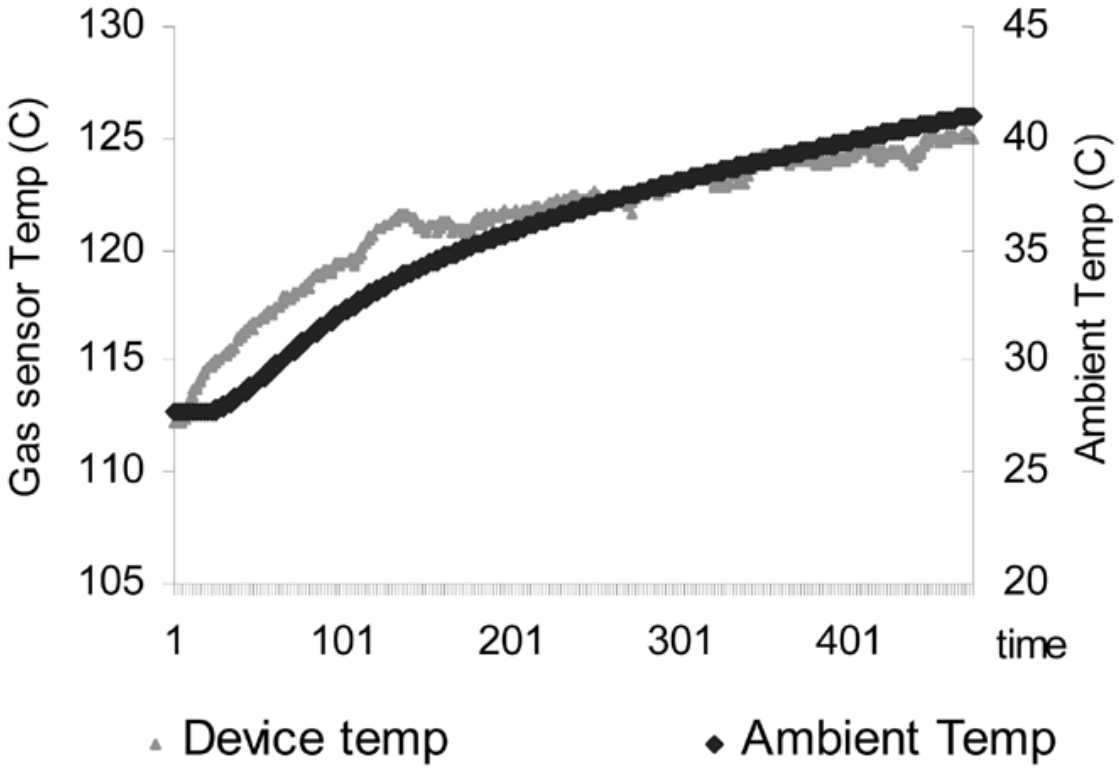

Figure 29: Ambient temperature effect on sensors' working temperature as a linear superposition [100]

According to the band bending theory mentioned in Chapter 2 the resistance of the tin oxide sensor can be expressed as [98],

$$R = R_O \exp(\frac{eV_S}{kT}) \qquad (28)$$

where R_O is the flat band resistance. The schottky potential barrier, V_S, in air is mainly controlled by the oxygen partial pressure and types of oxygen species adsorbed on the sensor surface [101]. According to the survey by Barsan and Weimar as shown in Figure 30 [102] in the testing temperature range O^- is dominant and has no significant change in types of oxygen species adsorbed on the sensor surface. Hence, there should not be a large change in Schottky potential barrier, V_S, as oxygen partial pressure can be regarded as constant at different temperatures during

the test.

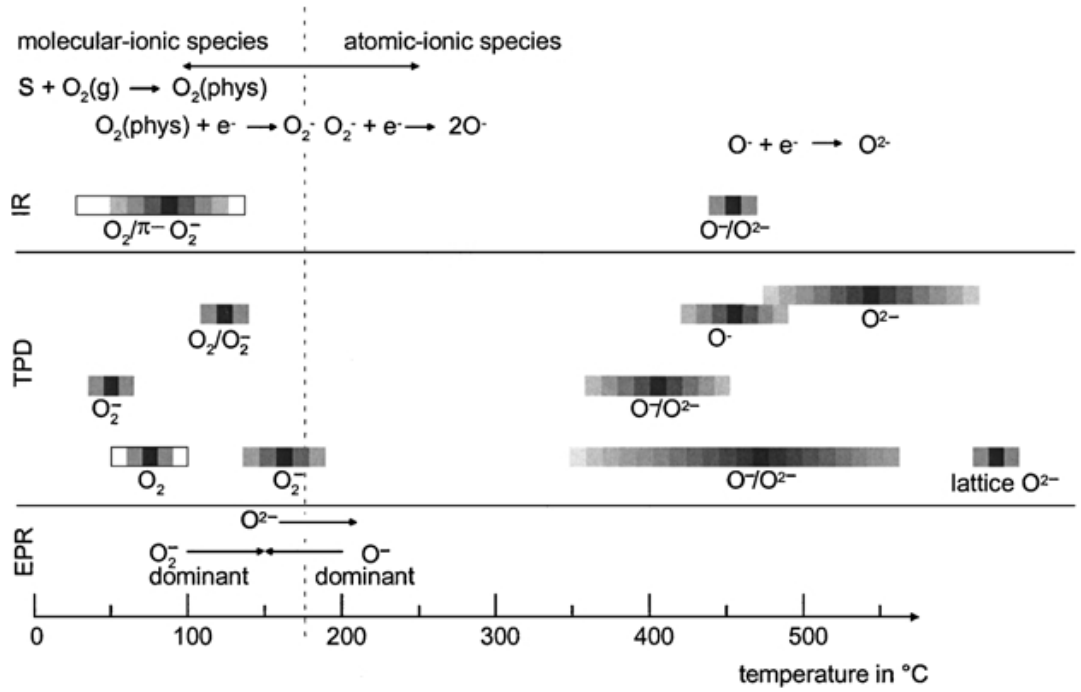

Figure 30: Survey of oxygen species detected at different temperatures at SnO2 surfaces with IR (infrared analysis), TPD (temperature programmed desorption), EPR (electron paramagnetic resonance) [102].

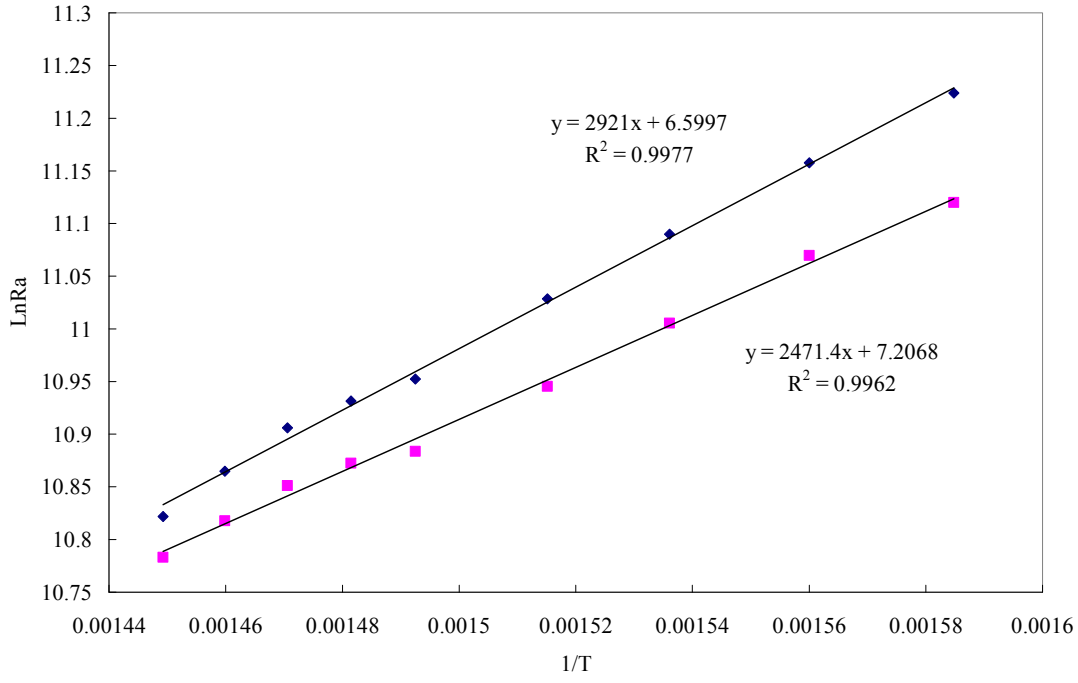

Figure 31: Sensors' logarithmic resistances in dry air at different temperatures.

By plotting the logarithmic resistances of the sensors in air verses inverse temperature of the sensor surface as shown in Figure 31, a linear relationship is obtained which is consistent with the theory.

The Schottky potential barrier, V_S, in reducing gases is very complex which is affected by adsorption and desorption rates of oxygen species and/or reducing gases or even reaction products, reaction rates between adsorbed oxygen species and reducing gases, charge carrier concentration and Debye length in the semiconductor [101]. The sensors' resistances are found to increase below 10°C, be almost constant between 10°C and 30°C and decrease above 30°C (Figure 27). It can be inferred that there are different mechanisms controlling the sensor resistance behavior in the testing temperature range.

5.3. Humidity dependence study

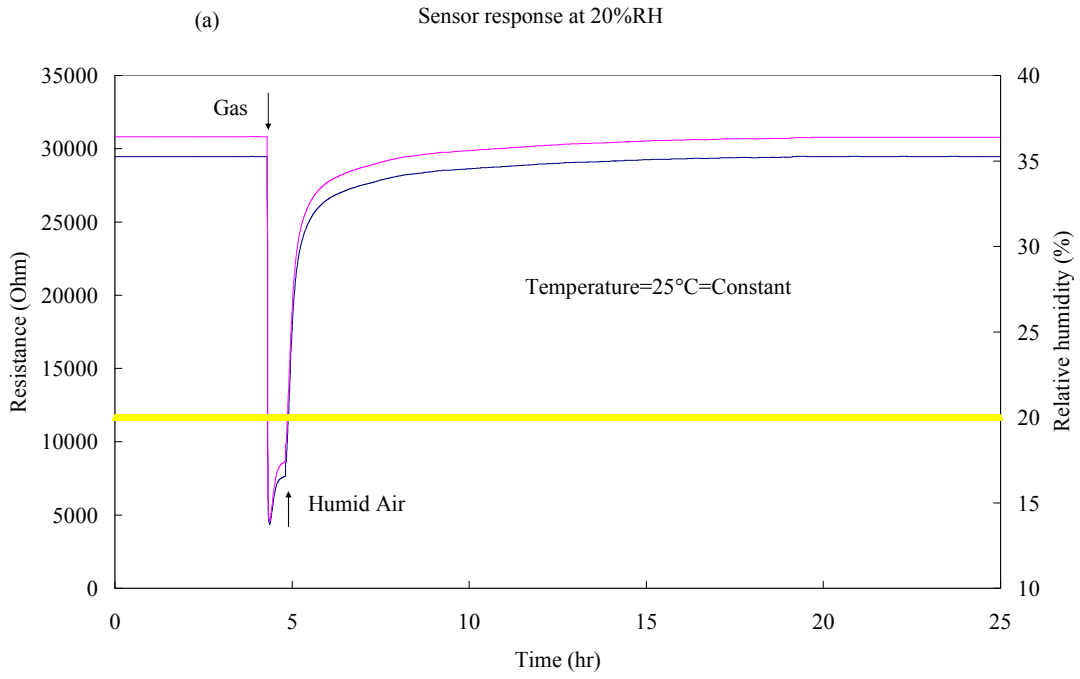

Figure 32a: Sensors' responses at relative humidity 20%.

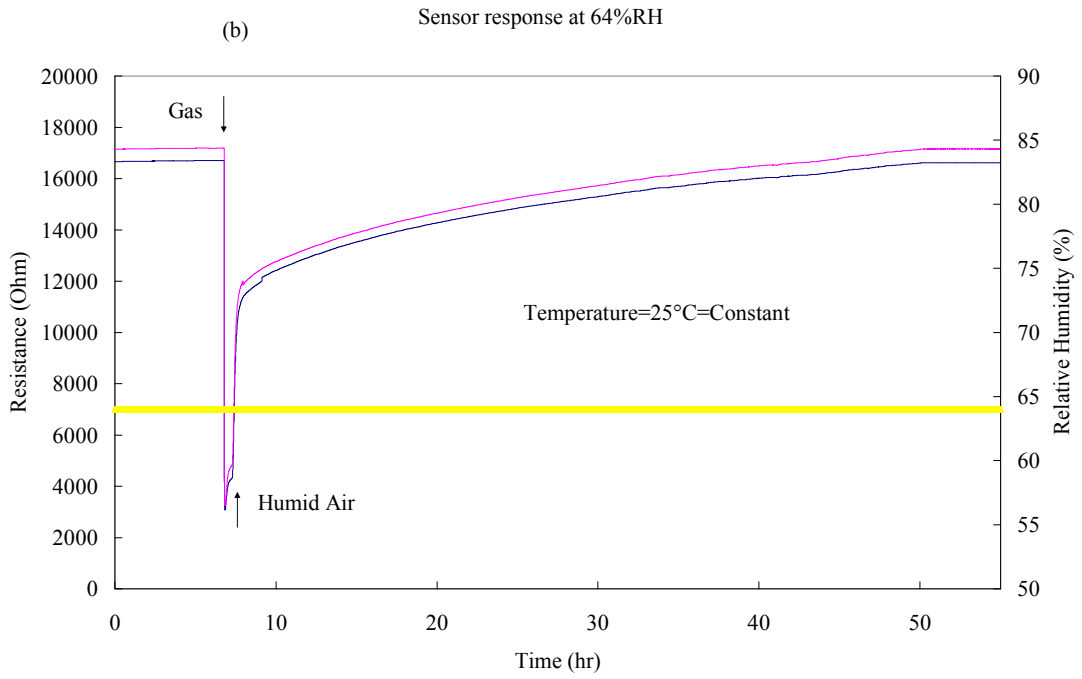

Figure 32b: Sensors' responses at relative humidity 64%.

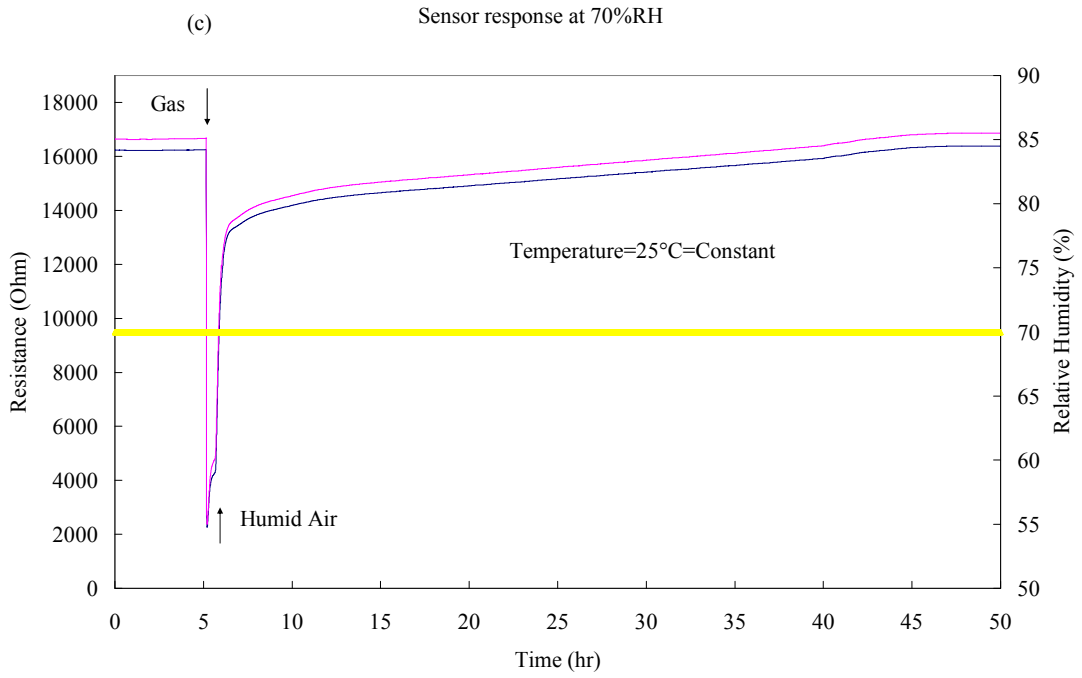

Figure 32c: Sensors' responses at relative humidity 70%.

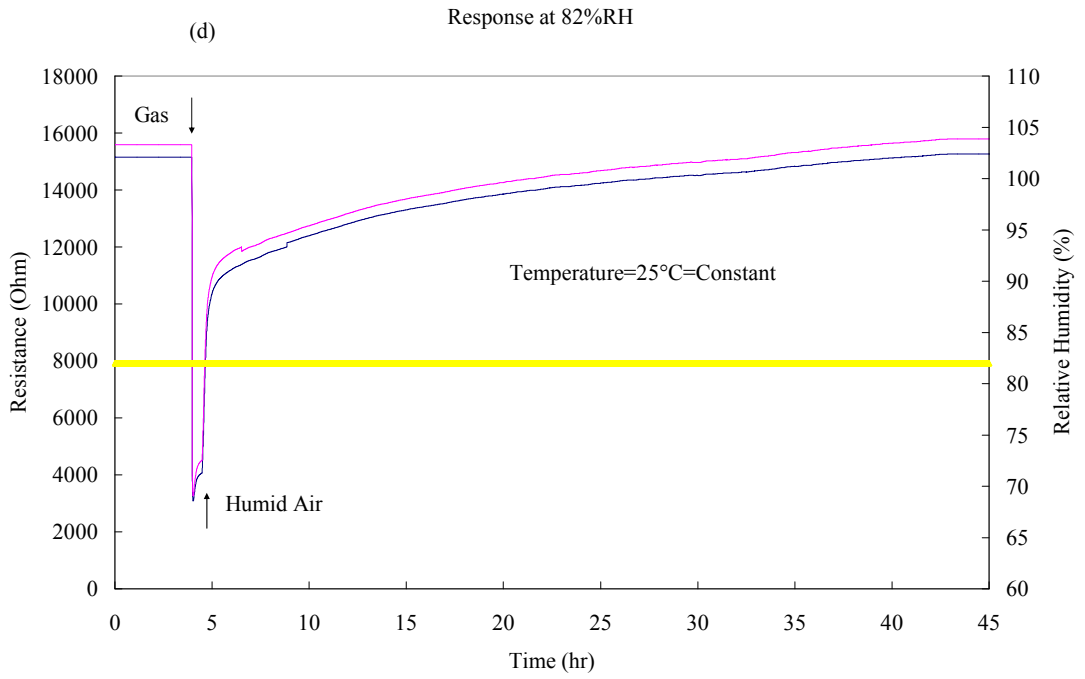

Figure 32d: Sensors' responses at relative humidity 82%.

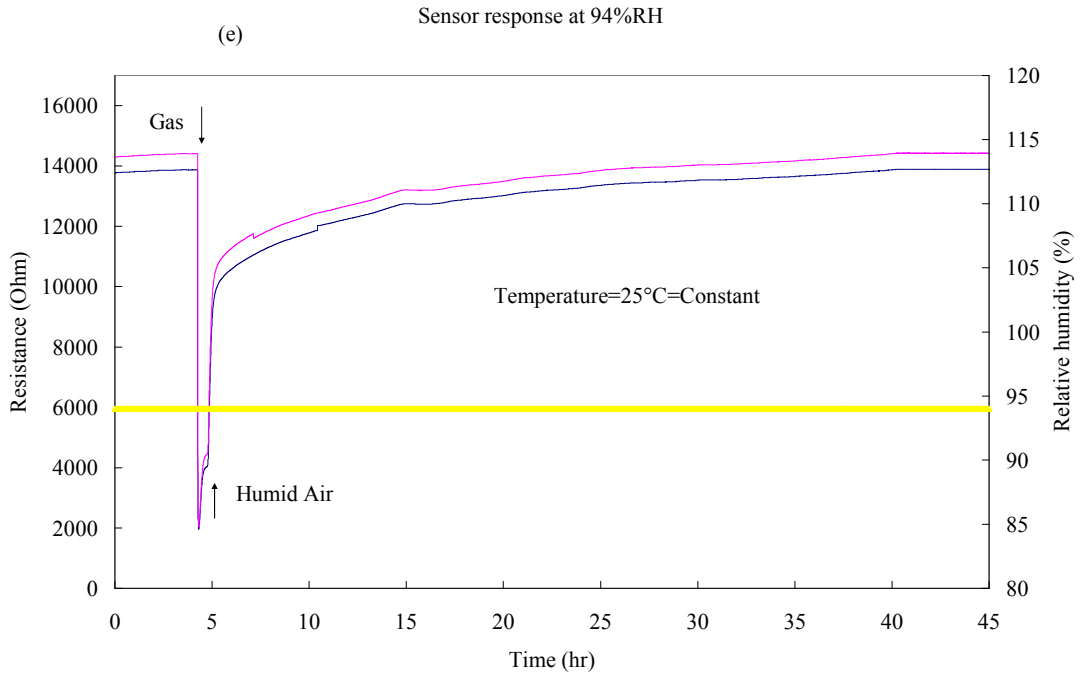

Figure 32e: Sensors' responses at relative humidity 94%.

Figure 32a to Figure 32e illustrate the sensors' responses at different relative

humidities. The thick line in the lower part of the figure is the relative humidity detected by the humidity sensor. The two thin lines are the resistances of two sensors. The flat initial resistances of the sensors and the ability to recover to initial resistances show good stability and reusability of the sensor at different relative humidities. The water vapor reduced the resistance of the sensor compared with in dry air. The sensors still respond to MeJa quickly and reach the lowest value in 4 minutes however they recover much slower than in dry air. They need more than 30 hours to recover to initial resistances in high relative humidity. The relative sensor response S is found to be decreasing with increasing relative humidity and decrease faster in high relative humidity (Figure 33).

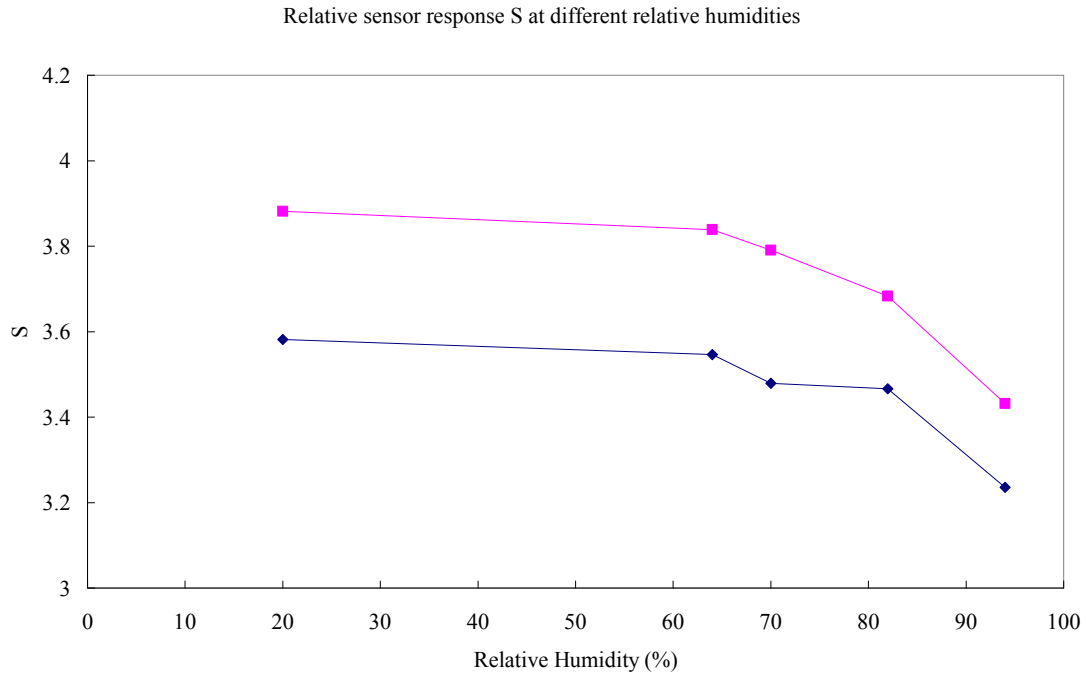

Figure 33: Relative sensor sensitivity S at different relative humidities.

By plotting the resistances of the sensors verses water vapor concentration in air on a logarithmic scale it was found that the sensors' resistances in humid air also follow the power law (Figure 34).

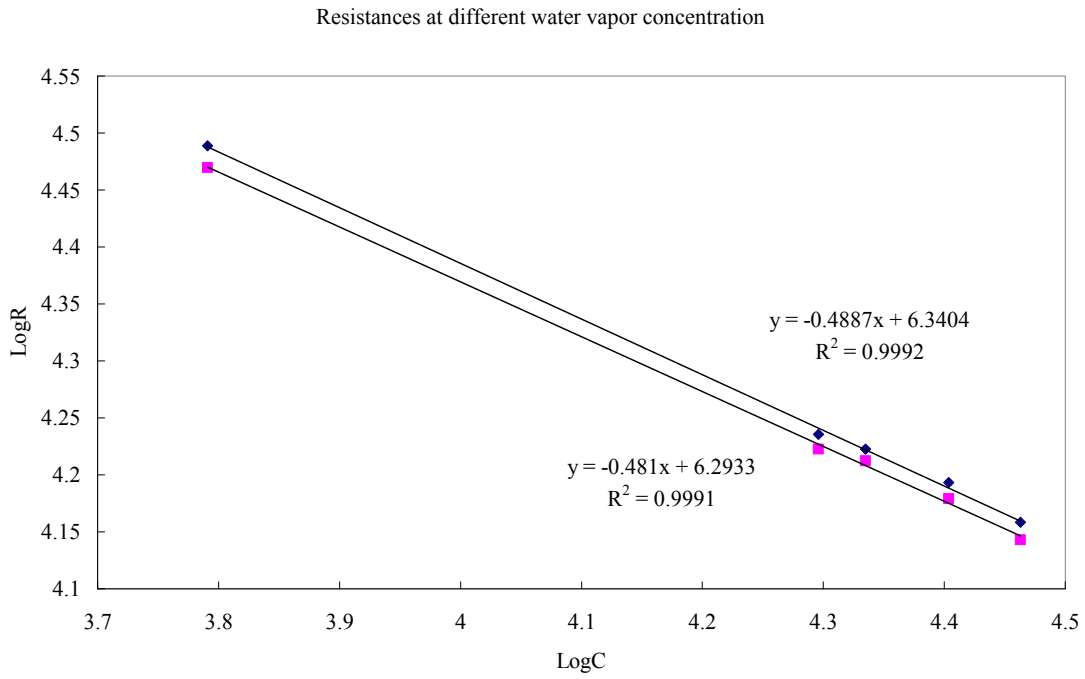

Figure 34: Sensors' initial resistances at different relative humidity.

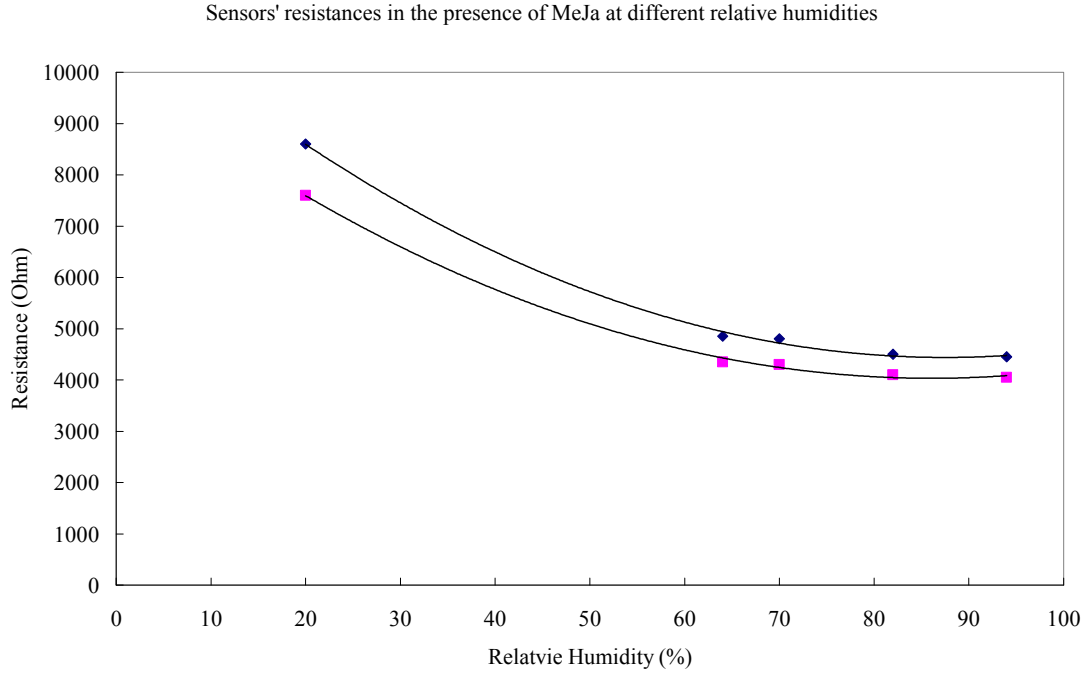

Figure 35: Sensors' resistances in the presence of MeJa at different relative humidities.

In the presence of MeJa the sensors' resistances decrease with increasing relative humidity but don't show the power law behavior (Figure 35). This means that water vapor contribution and the MeJa contribution to the reduction of the sensors' resistances are not independent of each other. Otherwise, the sensors' resistances at different relative humidity in the presence of MeJa should also follow the power law as the concentration of MeJa is fixed. However, it is not supported by the data. The reason for this is that the water vapor is competing with the reducing gases for preadsorbed oxygen species under different adsorption–desorption equilibrium conditions [103]. This also explains why the relative sensor response is decreasing with increasing relative humidity.

When the sensors are used in the field they can be distributed in different area. First, the baselines of the sensors are established at certain ambient temperature and humidity. When the ambient temperature and humidity changes the resistances of the sensors will gradually changes to corresponding status in a similar shape. If insects attack plants in some area, the volatile compounds which are emitted by plants change. The concentration of MeJa—an important defense system related chemical increases significantly in a short time. Hence, the resistances of the sensors in corresponding area should decrease quickly and have different resistance change shape from the sensors in other area. Thus, it can be used as a qualitative alarm for the insect infestation. The interfering effect of other volatile compounds is not tested this time and will be performed in future study.

CHAPTER 6: CONCLUSIONS

Thick film hotplate type tin oxide sensors can successfully detect Methyl Jasmonate and show good stability and reversibility at different ambient temperature and relative humidity. The sensors have a quick response to MeJa but the recover time of the sensor is very long, about 8 hours in dry air and even longer—more than 30 hours in high relative humidity. In the presence of MeJa from about 3ppm to 18ppm the relative sensor sensitivity S increases from 2 to 5 in dry air at ambient temperature 25°C and follow the power law. Sensors' resistances in dry air flow at different temperatures are proportional to 1/T on a logarithmic scale. Sensors' resistances in the presence of MeJa at different temperature in dry air flow are controlled by different dominant mechanisms in different testing temperature ranges. The relative sensor sensitivity in dry air flow is relatively low about 4 around ambient temperature 20°C and increases with decreasing ambient temperature below 10°C. Sensors' resistances in humid air flow at 25°C decrease with increasing water vapor concentration and also follow the power law. The relative sensor sensitivity decreases with increasing relative humidity and is still over 3 in high humidity.

By distributing the sensors in different area of the field, concentration change of MeJa can be qualitatively detected and discriminated from temperature and humidity changes. Hence, thick film type hotplate tin oxide sensor has great potential to be used as an in-situ qualitative alarm to the infestation of insects in site.

REFERENCES

[1] Chatterjee, Samprit, Biometrics 29 (1973), 727-734

[2] Massimo E. Maffei, Axel Mithofer, Wilhelm Boland, TRENDS in Plant Science 12 (2007) 7 310-316

[3] Ebel, J., Mithofer, Planta 206 (1998) 335–348

[4] White, P.J., BBA-Biomembranes 1465 (2000) 171–189

[5] Foyer, C.H., Noctor, G., Plant Cell Environ. 28 (2005) 1056–1071

[6] Asada, K., Plant Physiol, 141 (2006) 391–396

[7] Orozco-Ca′rdenas, M., Ryan, C.A., Proc. Natl. Acad. Sci. USA 96 (1999) 6553–6557

[8] Bennett, R.N. and Wallsgrove, R.M., New Physiologist 127 (1994)617-633

[9] Theis, N., Lerdau, M., International Journal of Plant Science 164 (2003) S93-S102

[10] Mao, J., Burt, A.J., Ramputh, A.-L., Simmons, J., Cass, L., Hubbard, K., Miller, S., Altosaar, I., Arnason, J.T., Journal of Agriculture and Food Chemistry 55 (2007) 2582-2589

[11] Jette T. Knudsen, Roger Eriksson, Jonathan Gershenzon, Bertil Ståhl, The Botanical Review 72(1) (2006) 1-120

[12] Natalia Dudareva, Florence Negre, Dinesh A. Nagegowda and Irina Orlova, Critical Reviews in Plant Sciences 25 (2006) 417–440

[13] Bernasconi, M. L., Turlings, T. C. J., Ambrosetti, L., Bassetti, P., Dorn S., Rhopalosiphum maidis. Entomol. Exp. Appl. 87 (1998) 133–142

[14] De Moraes, C. M., Mescheer, M. C., Tumlinson, J. H., Nature 410 (2001) 577–580

[15] Price, P. W., C. E. Bouton, P. Gross, B. A. McPheron, J. N. Thompson, A. E. Weis, Annual Review of Ecology and Systematics 11 (1980) 41–65

[16] Takabayashi, J., Dicke, M., Trends Plant Sci. 1 (1996) 109–113

[17] Dicke, M., Entomologia Experimentalis et Applicata 92 (1999b) 131–142

[18] Anderson, P., Alborn, H. Entomol. Exp. Appl. 92 (1999) 45–51

[19] Hilker, M., Meiners, T. Entomol. Exp. Appl. 104 (2002) 181–192

[20] Baldwin, I. T. & J. C. Schultz, Science 221 (1983) 277–279

[21] Rhoades, D. F., Recent Advances in Phytochemistry 19 (1985)195–218.

[22] Dicke, M., Abelis, M. W., Takabayashi, J., Bruin, J., Posthumus, M. A., J. Chem. Ecol. 16 (1990) 3091–3117.

[23] Arimura, G., Ozawa, R., Nishioka, T., Boland, W., Koch, T., Kuhnemann, F., Takabayashi, J., Plant J. 29 (2002) 87–98.

[24]Arimura, G., Ozawa, R., Kugimiya, S., Takabayashi, J., Bohlmann, J., Plant Physiol. 135 (2004b) 1976–1983

[25] Ruther, J., and Kleier, S., J. Chem. Ecol. 31 (2005) 2217–2222

[26] Green, T.R., Ryan, C.A. Science 175 (1972) 776-777

[27] Ussuf, K.K., Laxmi, N.H. and Mitra, R., Current Science, 80 (2001) 847-853

[28] Rawlings, N.D., Tolle, D.P. and Barrett, A.J., Biochemical Journal 378 (2005) 705-716

[29] Birgit Schulze, Ryan Lauchli, Mesmin Mekem Sonwa, Annika Schmidt, Wilhelm Boland, Analytical Biochemistry 348 (2006) 269–283

[30] Farmer EE, Johnson RR, Ryan CA. Plant Physiol 98 (1992) 995–1002

[31] Li L, Li C, Lee GI, Howe GA. 2002a. Proc Natl Acad Sci USA 99 (2002a) 6416–6421

[32] Fujita M, Fujita Y, Noutoshi Y, Takahashi F, Narusaka Y, Yamaguchi, Shinozaki

K, Shinozaki K, Curr Opin Plant Biol 9 (2006) 436-442

[33] Rojo E, Solano R, Sanchez-Serrano JJ, Plant Growth Regul 22 (2003) 82-98

[34] Tiryaki I, Staswick PE, Plant Physiol 130 (2002) 887-894

[35] Spoel SH, Koornneef A, Ctaessens SMC, Korzelus JP, Van Pelt JA, Mueller M J, Buchala A J, Metraux JP, Brown R, Kazzan K, Van Loon LC, Dong XN, Pieterse CMJ.. Plant Cell 15 (2003) 760-770

[36] Li J, Brader G, Palva ET., Plant Cell 16 (2004) 319-331

[37] Anderson JP, Badruzsaufari E, Schenk PM, Manners M, Desmond OJ, Ehlert C, Maclean D], Ebert PR, Kazan K, Pant Cell 16 (2004) 3460-3479

[38] Seo HS, Song JT, Cheong JJ, Lee Y-H, Lee YW, Hwang I, Lee JS, Choi YD Proc. Natl. Acad. Sci. U. S. A. 98 (2001) 4788–4793

[39] Jong-Joo Cheong and Yang Do Choi, TRENDS in Genetics 19 (2003) 409-413

[40] R. Karban, I.T. Baldwin, K.J. Baxter, G. Laue, G.W. Felton, Oecologia 125 (2000) 66–71

[41] Wasternack C, Hause B, Progr Nucl Acid Res Mol Biol 72 (2002) 165-221

[42] Riaan Meyer, George F. Rautenbach and Ian A. Dubery, Phytochemical. Analysis 14 (2003) 155–159

[43] N. Butt& L. Cinquegrani, E. Mugno, A. Tagliente and S. Pizzini, sensors and Actuators B, 6 (1992) 253-256

[44] Geraint Williams and Gary S. V. Coles, Sensors and Actuators 8, 15-16 (1993) 349-353

[45] Williams, E.W. Lawlor, C.M. Keeling, A.G. Gould, R.D., International Journal of Electronics, Vol. 76 Issue 5, May (1994) 815

[46] Ulrich Hoefer, Gerd Kühner, Werner Schweizer, Gerd Sulz, Klaus Steiner, Sensors and Actuators B 22 (1994) 115-119

[47] M. Di Giulio, G. Micocci, R. Rella, p. Siciliano, A. Tepore, Sensors and Actuators B 23 (1995) 193-195

[48] Ping Ping Tsai, I-Cherng Chen, Ming Hann Tzeng, Sensors and Actuators B 24-25 (1995) 537-539

[49] Klaus Steiner, Ulrich Hoefer, Gerd Kiihner, Gerd Sulz, Elmar Wagner, Sensors and Actuators B 24-25 (1995) 529-531

[50] Kiyoshi Fukui, Masanori Nakane, Sensors and Actuators B 24-25 (1995) 486-490

[51] Tadashi Mochida, Kei Kikuchi, Takehiko Kondo, Hironobu Ueno, Yoshinobu Matsuura, Sensors and Actuators B 24-25 (1995) 433-437

[52] G. Sarala Devi, S. Manorama, V.J. Rao, Sensors and Actuators B 28 (1995) 31-37

[53] W.K. Choi, S.K. Song, J.S. Cho, Y.S. Yoon, D. Choi, H., J. Jung, S.K. Koh, Sensors and Actuators B 40 (1997) 21-27

[54] Sang woo Lee, Ping ping Tsai, Haydn Chen, Sensors and Actuators B 41 (1997) 55-61

[55] V.A. Chaudhary, I.S. Mulla, S.R. Sainkar, A.A. Belhekar, K. Vijayamohanan, Sensors and Actuators A 65 (1998) 197-202

[56] Jae Chang Kim, Hee Kwon Jun, Jeung-Soo Huh, Duk Dong Lee, Sensors and Actuators B 45 (1997) 271–277

[57] V.N. Mishra, R.P. Agarwal, Microelectronics Journal 29 (1998) 861-874

[58] Zhihong Jin, Huan-Jun Zhou, Zhang-Li Jin, Robert F. Savinell, Chung-Chiun Liu, Sensors and Actuators B 52 (1998) 188–194

[59] A. Katsuki, K. Fukui, Sensors and Actuators B 52 (1998) 30–37

[60] A. Chaturvedi, V.N. Mishra, R. Dwivedi, S.K. Srivastava, Microelectronics

Journal 30 (1999) 259–264

[61] V.A. Chaudhary, I.S. Mulla, K. Vijayamohanan, Sensors and Actuators B 55 (1999) 154–160

[62] M.C. Horrillo, I. Sayago, L. Are´s, J. Rodrigo, J. Gutie´rrez, A.Go¨tz, I. Gra`cia, Fonseca, C. Cane, E. Lora-Tamayo, Sensors and Actuators B 58 (1999) 325–329

[63] Go Sakai, Nam Seok Baik, Norio Miura, Noboru Yamazoe, Sensors and Actuators B 77 (2001) 116-121

[64] Yu-De Wang, Chun-Lai Ma, Xing-Hui Wu, Xiao-Dan Sun, Heng-De Li, Sensors and Actuators B: Chemical 85 (2002)270-276

[65] K. Anothainart, M. Burgmair, A. Karthigeyan, M. Zimmer, I. Eisele, Sensors and Actuators B 93 (2003) 580–584

[66] S. Shukla, S. Patil, S.C. Kuiry, Z. Rahman, T. Du, L. Ludwig, C. Parish, S. Seal, Sensors and Actuators B 96 (2003) 343–353

[67] Behzad Esfandyarpour, Shams Mohajerzadeh, Abbas Ali Khodadadi, and Michael D. Robertson, IEEE SENSORS JOURNAL, 4 (2004) 449-454

[68] S.M.A. Durrani, E.E. Khawaja, M.F. Al-Kuhaili, Talanta 65 (2005) 1162–1167

[69] U lo Kersen, Lauri Holappa, Analytica Chimica Acta 562 (2006) 110–114

[70] Satyajit Shukla, Peng Zhang, Hyoung J. Cho, Sudipta Seal, Lawrence Ludwig, Sensors and Actuators B 120 (2007) 573–583

[71] Yun-Hyuk Choi, Seong-Hyeon Hong, Sensors and Actuators B 125 (2007) 504–509

[72] Chang Sup Moon, Hae-Ryong Kim, Graeme Auchterlonie, John Drennan, Jong-Heun Lee, Sensors and Actuators B 131 (2008) 556–564

[73] Jun Zhang, ShurongWang, YanmeiWang, YanWang, Baolin Zhu, Huijuan Xia, Xianzhi Guo, Shoumin Zhang,Weiping Huang, ShihuaWu, Sensors and Actuators B

135 (2009) 610–617

[74] Cesar Elosua, Ignacio R. Matias, Candido Bariain and Francisco J. Arregui, Sensors, 6 (2006)1440-1465

[75] Alexander P. Demchenko, Introduction to Fluorescence Sensing, Springer (2009)

[76] Jiri Homola, Sinclair S. Yee a, Gunter Gauglitz, Sensors and Actuators B 54 (1999) 3–15

[77] P. T. Moseley and B. C. Tofield, Solid State Gas Sensors, (1987) Adam Hilger, Bristol

[78] Deng Y, Nevell T G, Ewen R J, Honeybourne C L, Appl Catal A-Gen, 101 (1993) 51

[79] L. A. Obvintseva,, Russian Journal of General Chemistry, 78, (2008) 2545–2555

[80] Hua Bai and Gaoquan Shi, Sensors, 7 (2007) 267-307

[81] P. Pasierb, M. Rekas, J Solid State Electrochem, 3 (2009) 3–25

[82] C. O. Park, J. W. Fergus , N. Miura, Jinsu Park, Angi Choi, Ionics, 15 (2009) 261–284

[83] Stetter, J. R.; Chang, S. C.; Cha, C. S. Talanta, 40, (1993) 461-477

[84] David James, Simon M. Scott, Zulfiqur Ali, William T. O'Hare, Microchim. Acta 149, (2005) 1–17

[85] Ralf Lucklum . Peter Hauptmann, Anal Bioanal Chem, 384 (2006) 667–682

[86] P.T. Moseley, Meas. Sci. Technol. 8 (1997) 223–237

[87] S. Capone, A. Forleo, L. Francioso, R. Rella, P. Siciliano, J. Spadavecchia, D.S. Presicce, A.M. Taurino, J. Optoelectr. Adv. Mater. 5 (5) (2003) 1335–1348

[88] G. Korotcenkov, Materials Science and Engineering B 139 (2007) 1–23

[89] C. O. Park, S. A. Akbar, Journal of Materials Science 38 (2003) 4611 – 4637

[90] Matthias Batzill, Ulrike Diebold, Progress in Surface Science 79 (2005) 47–154

[91] P . B. WEISZ, J. Chem. Phys. 21 (1953) 1531

[92] P. K. Clifford, D. T. Tuma, Sensors and Actuators, 3 (1983) 233-254.

[93] J Watson, Sensors and Actuators, 5 (1984) 29 – 42

[94] Shigeki Hirobayashi, Mohammed Afrose Kadir, Toshio Yoshizawa, Tatsuo Yamabuchi, Sensors and Actuators B 92 (2003) 269–278

[95] Williams D E 1987 Conduction and gas response of semiconductor gas sensors in Solid State Gas Sensors ed P T Moseley and B C Tofield (Bristol: Adam Hilger) 71

[96] G. Sberveglieri, S. Groppelli, P. nelli ,Sensors and Actuators B, 4 (1991) 457-461

[97] Rajeev K. Srivastava, P. Lal, R. Dwivedi, SK. Srivastava, Sensors and Actuators B 21 (1994) 213-218

[98] G. Martinelli, M.C. Carotta, Sensors and Actuators B 23 (1995) 157-161

[99] Noboru Yamazoe, Kengo Shimanoe, Sensors and Actuators B 128 (2008) 566–573

[100] Jian-Wei Gong, Quan-Fang Chen, Ming-Ren Lian, Nen-Chin Liu, Claude Daoust, IEEE SENSORS JOURNAL, 6 (2006) 139-145

[101] Andrew P. Lee, Brian J. Reedy, Sensors and Actuators B 60 (1999) 35–42

[102] Nicolae Barsan, Udo Weimar, Journal of Electroceramics, 7 (2001) 143–167

[103] Dorota Koziej, Nicolae Baˆrsan, Udo Weimar, Jacek Szuber, Kengo Shimanoe, Noboru Yamazoe, Chemical Physics Letters 410 (2005) 321–323